SILVER IONS BONDING ON POLYPROPYLENE BY UNDERWATER DOUBLE DIAPHRAGM DISCHARGE FOR ANTIMICROBIAL APPLICATIONS

GABRIELA NEAGOE*[a], ANTONÍN BRABLEC[a], JOZEF RÁHEĽ[a,b], VILMA BURŠÍKOVÁ[a,c]

[a] *Dep. of Physical Electronics, Faculty of Science, Masaryk University, Kotlářská 2, 611 37 Brno, Czech Republic,* [b] *Dep. of Experimental Physics, Comenius University, Mlynská dolina F2, 842 48 Bratislava, Slovak Republic,* [c] *CEITEC - Central European Institute of Technology, MU, 601 77 Brno, Czech Republic*
gabriela.pirpiliu@yahoo.com

Keywords: underwater discharge, antibacterial effect, silver, polypropylene

1. Introduction

Production of technical textiles is one of the fast growing sectors of the global textile industries. Textile materials used in the medical, health care and hygiene sectors are an important and expanding part of the industry, and they are usually referred to as biomedical textiles. This group of products demonstrates a great range of applications, from simple bandages to biocompatible implants and tissues; antibacterial wound treatment material, prosthetics and so called intelligent textiles.

The application of nonwoven fabrics varied in the wide range from hygienic products to medical fabrics and industrial applications. By appropriate surface treatments nonwoven polypropylene (PP) can be advanced in the biocompatible fabric and can acquire antimicrobial properties. Moreover, a new generation of dressing incorporating antimicrobial agents like silver and iodine has been studied[1].

For this study we used the underwater discharge generated in a diaphragm electrode configuration as the treatment technique for the PP nonwoven in a solution of silver salt ($AgNO_3$). Silver is a non-toxic, non-tolerant disinfectant that can significantly reduce many bacterial infections[2,3]. Bacteria have different membrane structures which allow a general classification of them as Gram-negative or Gram positive. The structural differences lie in the organization of a key component of the membrane, peptidoglycan. Gram negative bacteria exhibit only a thin peptidoglycan layer (~2–3 nm) between the cytoplasmic membrane and the outer membrane[4]; in contrast, Gram-positive bacteria lack the outer membrane but have a peptidoglycan layer of about 30 nm thick[5].

The possibility of combining the plasma chemical activity with the selectivity of processes in solutions[6] is an advantage of the discharge in water. It produces effectively hydrated electrons and hydroxyl radicals which can be used for material surface modification[7,8]. The obtained results indicate the unique capability of the underwater diaphragm discharge to activate the fabric and immobilize the particles on fibers surface within a single process step.

2. Experimental setup

The electrodes were connected to a pulsed HV power supply based on the double rotating spark gap. The maximum peak voltage was 40 kV DC. The maximum repetitive rate of pulses was 60 Hz. The duration of the electrical pulses was determined by the water conductivity. The distance between the diaphragms was 13 cm (Fig. 1).

Double diaphragm discharge is improving the treatment uniformly.

Polypropylene nonwoven fabrics of 50 grams per square meter (gsm) and 30 mm width supplied by PEGAS NONWOVENS s.r.o. (Czech Republic), was fed trough the slit with an adjustable speed. After treatment the samples were washed in a detergent solution in an ultrasonic bath for 20 minutes in order to remove weakly attached silver mictoparticles.

3. Results and discussion

The „Determination of antibacterial activity – Agar diffusion plate test“ method was used to study the antibacterial properties of the PP nonwoven textile.

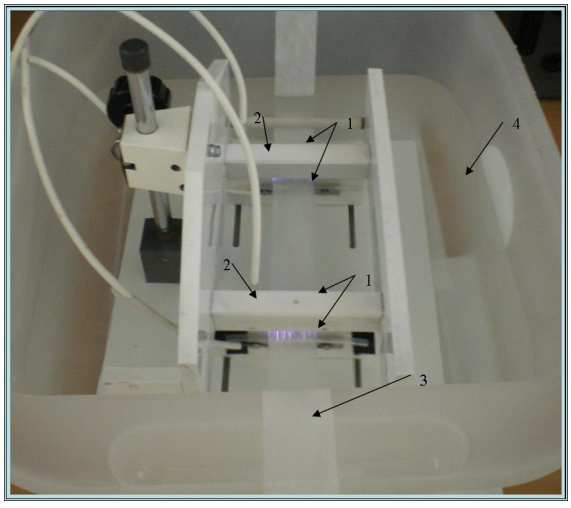

Fig. 1. **Experimental arrangement for Double Diaphragm Discharge:** 1 – electrodes; 2 – diaphragm; 3 – polypropylene nonwoven fabric; 4 – water-based solution

The samples were placed on a germ-containing agar plate and were inoculated with Gram-positive (*Staphylococcus aureus*) bacteria and Gram-negative (*Escherichia coli*) bacteria. In the images presented in Fig. 2 and Fig. 3, we can observe the antimicrobial effect of the washed and unwashed treated PP fabric against *S. aureus* and *E. coli*.

The antibacterial properties of the treated PP in solution of silver salt against *S. aureus* and *E. Coli* are presented in Tab. I and Tab. II.

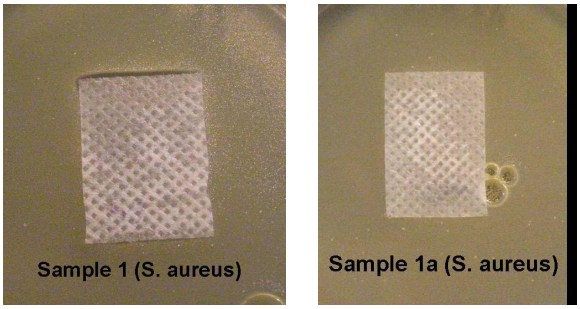

Fig. 2. **Images of the unwashed (sample 1) and washed (sample 1a) samples effect on *Staphylococcus aureus* bacteria**

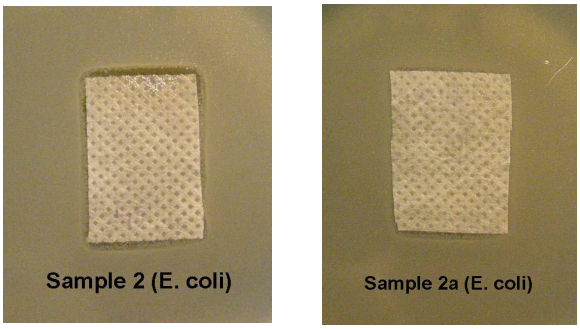

Fig. 3. **Images of the unwashed (sample 2) and washed (sample 2a) samples effect on *Escherichia coli* bacteria**

Table I
Antibacterial properties of the treated PP against *S. aureus*

Sample	Growth[a)]	Assessment
Ref – only PP	heavy	insufficient effect[b)]
Sample 1	none (inhibition zone = 0.5 mm)	good effect[c)]
Sample 1a (after washing)	none	good effect

[a] The growth of bacteria in the nutrient medium under the specimen, [b] no inhibition zone, compared to the control no growth reduction therefore insufficient effect, [c] no growth, the inhibition zone exceeding 1 mm or up to 1 mm (good effect)

Table II
Antibacterial properties of the treated PP against *E. coli*

Sample	Growth	Assessment
Ref – only PP	heavy	insufficient effect
Sample 2	none (inhibition zone = 1mm)	good effect
Sample 2a (after washing)	none	good effect

Samples 1a and 2a presented no inhibition zone and no growth of bacteria under the specimen. These samples were washed with detergent in an ultrasound bath for 20 min, as mentioned before. Samples 1, 2 (before washing) indicate an inhibition zone up to 1 mm and no growth of bacteria under the specimen. In case of the untreated PP, no inhibition zone and no growth reduction under the specimen were observed.

Fig. 4 and Fig. 5 show SEM micrographs of one of the treated samples in water solution of silver salt (σ = 6.54 mS cm^{-1}) before and after washing.

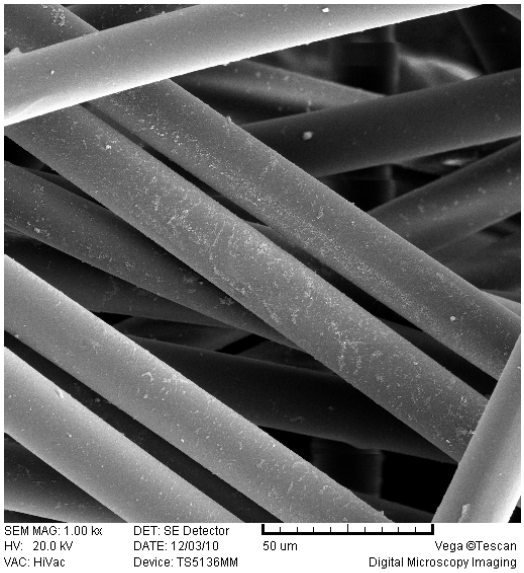

Fig. 4. **SEM micrographs of the sample treated in silver salt solution before washing**

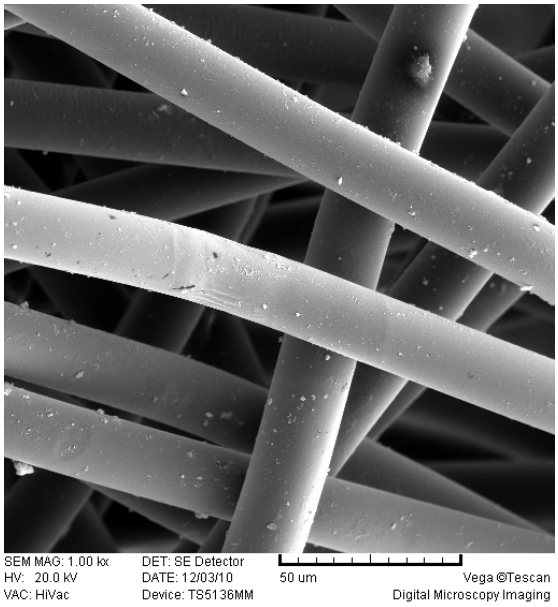

Fig. 5. **SEM micrographs of the sample treated in silver salt solution after washing**

From the Scanning Electron Microscop (SEM) images we can observe that the particles were not removed during washing and are uniformly spread on the textile surface, on both washed and unwashed samples.

The Energy Dispersive X-ray (EDX) analysis confirmed the presence of silver on the PP surface and no peaks of other impurities were detected. Similar results were obtained in different places on the samples.

4. Conclusion

SEM micrographs indicated that the silver crystals are well dispersed on the PP textile and the washing test confirmed that the particles are quite durably immobilized on the fibers surface. The EDX analysis confirmed the nature of the silver on the PP surface.

Performing Double Diaphragm discharge in the water solution of silver salt, we were able to immobilize the salts crystals on the surface of PP fibers. The „determination of antibacterial activity – Agar diffusion plate test" confirmed a good antimicrobial effect of PP nonwoven fabric with the immobilized salts crystals (no growth under the specimen and an inhibition zone up to 1 mm).

The observed antimicrobial effect for *S. aureus* and *E. coli* together with the fact that even after washing the fabric in ultrasonic bath the salt crystals are still attached on the fiber surface indicate that the Double Diaphragm discharge can be used advantageously for manufacturing of antimicrobial PP nonwovens in a single processing step.

This research has been supported by the Czech Science Foundation under the contact numbers 202/09/2064 and 104/09/H080 as well as by the project CZ.1.05/2.1.00/03.0086 'R&D center for low-cost plasma and nanotechnology surface modifications' funded by European Regional Development Fund.

REFERENCES

1. Schaller M., Laude J., Bodewaldt H., Hamm G., Korting H. C.: Skin Pharmacol. Physiol. *17*, 31 (2004).
2. Nakashima T., Sakagami Y., Ito H., Matsuo M.: Textile Res. J. *71*, 688 (2001).
3. Klaus-Joeger T., Joeger R., Olsson E., Granqvist C. G.: Trends Biotechnol. *19*, 15 (2001).
4. Murray R. G. E., Steed P., Elson H. E.: Can. J. Microbiol. *11*, 547 (1965).
5. Shockman G. D., Barret J. F.: Annu. Rev. Microbiol. *37*, 501 (1983).
6. Joshi R., Schulze R. D., Meyer-Plath A., Friedrich J. F.: Plasma Process. Polym *5*, 695 (2008).
7. Brablec A., Slavicek P., Stahel P., Cizmar T., Trunec D., Simor M., Cernak M.: Czech. J. Phys. *52* Suppl. D491 (2002).
8. Simor M., Krump H., Hudec I., Rahel J., Brablec A., Cernak M.: Acta Physica Slovaca *54*, 43 (2004).

G. Neagoe[a], A. Brablec[a], J. Ráhel'[a,b], and V. Buršíková[a,c] *([a] Dep. of Physical Electronics, Faculty of Science, Masaryk University, Brno, Czech Republic; [b] Dep. of Experimental Physics, Comenius University, Bratislava, Slovak Republic, , [c] CEITEC - Central European Institute of Technology, MU, Brno, Czech Republic):* **Silver Ions Bonding on Polypropylene by Underwater Double Diaphragm Discharge for Antimicrobial Applications**

An underwater plasma discharge is used for surface activation of polypropylene fabrics with subsequent immobilisation of silver particles. The „Textile fabrics – Determination of antibacterial activity – Agar diffusion plate test" was used to study the antibacterial properties of the treated PP nonwoven textile against *S. aureus* and *E. coli* bacteria. Distribution of the dispersed particles were measured by Scanning Electron Microscopy (SEM) and the chemical nature of crystals was confirmed by the Energy Dispersive X-ray (EDX) analysis of the sample.

ANTIBACTERIAL EFFECT OF COPPER IONS BONDED ON POLYPROPYLENE NONWOVEN BY UNDERWATER DOUBLE DIAPHRAGM DISCHARGE

GABRIELA NEAGOE*[a], ANTONÍN BRABLEC[a], ANNA ZÁHORANOVÁ[b], VILMA BURŠÍKOVÁ[a,c]

[a] *Dep. of Physical Electronics, Faculty of Science, Masaryk University, Kotlářská 2, 611 37 Brno, Czech Republik,* [b] *Dep. of Experimental Physics, Comenius University, Mlynská dolina F2, 842 48 Bratislava, Slovak Republik,* [c] *CEITEC - Central European Institute of Technology, MU, 601 77 Brno, Czech Republic*
gabriela.pirpiliu@yahoo.com

Keywords: underwater discharge, PP nonwoven, copper, antibacterial properties

1. Introduction

Underwater electrical discharges systems attract the attention of many research groups mainly for its proven eficiency in the wastewater remediations[1]. Recently emerged application for underwater electrical discharge offering a substantial economical and enviromental benefits compared with conventional wet chemical methods is the surface functionalization of textile materials (for example acid processing and alkaline hydrolysis)[2]. Only a small number of works has been published devoted to materials treatment by underwater plasma[3,4].

Underwater discharges generated in water solutions are effective sources of OH radicals, solvated electrons and number of others active species[5,6]. It is known that OH radicals can be used to incorporate hydroxyl groups in the structure of polymer materials, predominantly into polyaromatic polymers[7]. Together with solvated electrons OH radicals can take part in the formation of secondary active species such as H_2O_2, and O_3 which are strong oxidation and bleaching agents[1]. The aim of this work is to estimate the possibility of application of double diaphragm discharge system to processes of textile material treatment, and to evaluate the bactericidal effect of the polypropylene (PP) nonwoven treated in water solution of copper salt on *Staphylococcus aureus*.

The excellent physical and chemical properties of polypropylene (chemical resistance, low density, highest melting point in the family of olefin fibers, and moderate cost), compared to other fibers, make it an important fiber, increasingly used in industrial application.

Copper ions, either alone or in copper complexes, have been used for centuries to disinfect liquids, solids and human tissue. Bonding copper on polypropylene fibers or other polymeric materials enable the production of clothing, bedding and medical devices that possess biocidal properties.

In comparison with other methods, in the underwater diaphragm discharge we activate the surface and immobilize the particles in the same time.

2. Experimental setup

The discharge was generated in a narrow slit of 0.1×1×40 mm positioned between two metallic electrodes at 2 cm mutual distance. The distance between the diaphragms is 13 cm. The electrodes were connected to a pulsed HV power supply based on the double rotating spark gap. The maximum peak voltage was 40 kV DC. The maximum repetitive rate of pulses was 60 Hz. The duration of the electrical pulses was determined by the water conductivity.

The schematic of experimental setup is shown in Fig. 1.

The interfacial bonding between the particles and the PP fibers was observed by Scanning Electron Microscopy

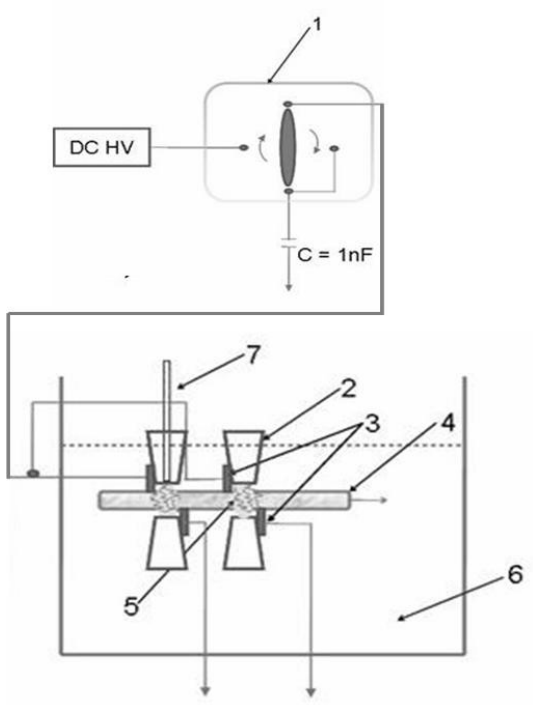

Fig. 1. **Double diaphragm discharge:** 1 – rotating spark gap; 2 – diaphragm; 3 – electrodes; 4 – textile; 5 – plasma; 6 – water solution; 7 – optical fiber

(SEM). The surface chemical compositions were analyzed by Energy Dispersive X-ray (EDX).

The ISO 20645 „Textile fabrics – Determination of antibacterial activity – Agar diffusion plate test“ was used to study the antibacterial properties of the PP nonwoven textile. The samples (treated and untreated) were placed on a germ-containing agar plate and were inoculated with Gram-positive (*Staphylococcus aureus*, ATCC 6538) bacteria. For this test i tis very important to have no growth of bacteria under the specimen and for better results also around the specimen (the so called inhibition zone).

3. Results and discussion

The polypropylene was treated in water solutions of $CuSO_4$, with different conductivities. Polypropylene nonwoven fabric of 50 gsm (grams per square meter) and 30 mm width was fed through the slit with an adjustable speed. After treatment we washed the sample in a detergent solution in Ultrasonic Bath for 15 minutes to see how many particles remain attached to the textile material.

Fig. 2 and Fig. 3 show SEM micrographs of one of the treated samples in water solution copper salt ($CuSO_4$) (σ = 6.73 mS cm^{-1}) before and after washing. We can observe that the particles were not removed during washing and are spread on the textile surface, on both washed and unwashed samples. Comparing the SEM micrographs of several samples, in different places on each sample, we observed that more than 70 % of these crystals were still attached even after the intense washing.

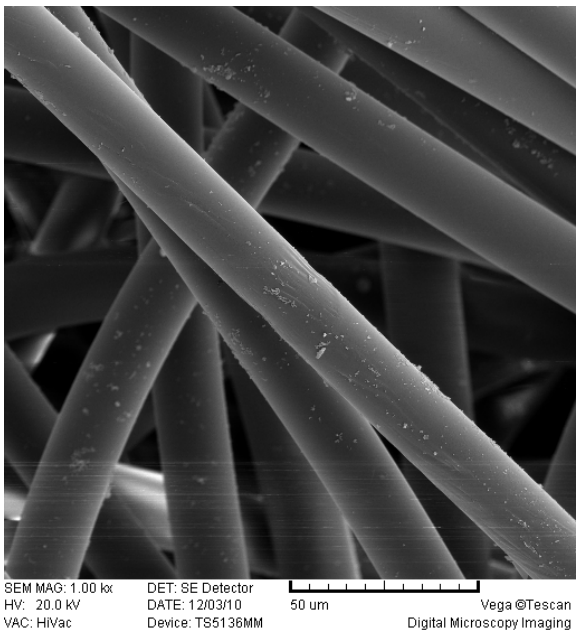

Fig. 2. **SEM micrographs of one spot on the sample treated in copper salt solution before washing**

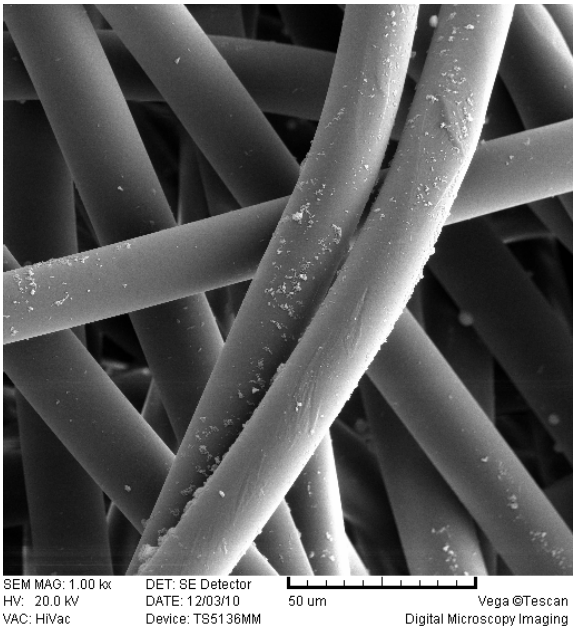

Fig. 3. **SEM micrographs of one spot on the sample treated in copper salt solution after washing**

The EDX analysis confirmed the presence of elemental cooper on the fabric fibers surface. Except the Au peak that appeared because of the initial coating of the samples with gold, no peaks of other impurities were detected.

In the image presented in Fig. 4, we can observe the different antimicrobial effect of the washed and unwashed treated PP fabric. Samples 11a and 12a (after washing) presented no inhibition zone and no growth of bacteria under the specimen. Sample 12 (before washing) indicate an inhibition zone up to 1 mm and no growth of bacteria under the specimen. In case of the untreated PP, no inhibition zone and no growth reduction under the specimen were observed.

Tab. I shows the antibacterial properties of the fabrics treated in solution of copper salt, where a) represents the growth of bacteria in the nutrient medium under the specimen, b) no inhibition zone, compared to the control no growth reduction therefore insufficient effect, c) no growth, the inhibition zone exceeding 1mm or up to 1 mm (good effect). All of the specimens exhibited excellent percentage reductions against *S. aureus*.

The assessment is based on the absence or presence of bacterial growth in the contact zone between agar and specimen and on the eventual appearance of an inhibition zone around the specimens.

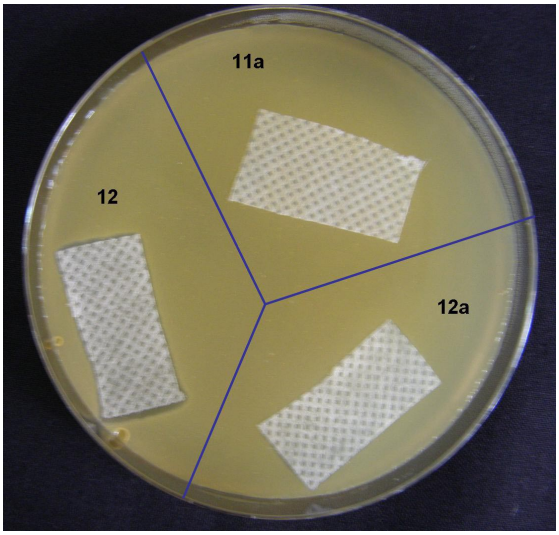

Fig. 4. **Photographic image of the incubation of *Staphylococcus aureus* on the nonwoven fabric after 24 h**: (sample 12) treated in solution of copper salt before washing; (sample 11a and 12a) after washing in ultrasound bath for 15 min

4. Conclusion

Our results indicated that underwater diaphragm plasma can immobilize copper crystals on the PP surface, copper being well known for its antibacterial properties. The „determination of antibacterial activity – Agar diffusion plate test" confirmed the antimicrobial effect of PP nonwoven fabric treated in $CuSO_4$ solution by underwater double diaphragm discharge against *S. aureus* (no growth under the specimen and an inhibition zone up to 1 mm). Also the fact that even after washing the fabric in ultrasonic bath the copper particles are covering more than 70 % of the fiber surface, allows us to consider that the diaphragm discharge can be potentially used in biomedical applications.

Table I
Antibacterial properties of the treated fabrics

Sample	Growth[a]	Assessment
Ref – only PP	heavy	insufficient effect[b]
11a (after washing)	none	good effect[c]
12	inhibition zone (1 mm)	good effect
12a (after washing)	none	good effect

This research has been supported by the Czech Science Foundation under the contact numbers 202/09/2064 and 104/09/H080 as well as as well as by the project CZ.1.05/2.1.00/03.0086 'R&D center for low-cost plasma and nanotechnology surface modifications' funded by European Regional Development Fund.

The work was also the result of the project implementation 26240220042 supported by the Research & Development Operational Programme funded by the ERDF.

REFERENCES

1. Locke B. R., Sato M. et al.: Ind. Eng. Chem. Res. *45*, 882 (2006).
2. Pastore Ch. M., Keikens P.: *Surface characteristics of fiber and textile*. *Surface science series*. *94*, New York – Basel, 2001.
3. Brablec A., Slavicek P., Stahel P., Cizmar T., Trunec D., Simor M., Cernak M.: Czech. J. Phys. *52* Suppl. D491 (2002).
4. Simor M., Krump H., Hudec I., Rahel J., Brabec A., Cernak M.: Acta Physica Slovaca *54*, 43 (2004).
5. Sunka P.: Physics of Plasmas *8*, 2587 (2001).
6. Malik M. A., Ghaffar A. Malik S. A.: Plasma Sources Sci. Technol. *10*, 82 (2001).
7. Steen M. L., Butoi C. I., Fisher E. R.: Langmuir *17*, *26*, 8156 (2001).

G. Neagoe[a], A. Brablec[a], A. Zahoranová[b], and V. Buršíková[a,c] *([a] Dep. of Physical Electronics, Faculty of Science, Masaryk University, Brno, Czech Republic; [b] Dep. of Experimental Physics, Comenius University, Bratislava, Slovak Republic, [c] CEITEC - Central European Institute of Technology, MU, Brno, Czech Republic):* **Antibacterial Effect of Copper Ions Bonded on Polypropylene Nonwoven by Underwater Double Diaphragm Discharge**

Underwater plasma discharge was used for surface activation of polypropylene fabrics with subsequent immobilisation of copper particles. Size and distribution of dispersed particles were measured by Scanning Electron Microscopy (SEM) and the chemical nature of crystals was confirmed by the Energy Dispersive X-ray (EDX) analysis of the sample. „Determination of antibacterial activity – Agar diffusion plate test" method was used to study the antibacterial properties of the PP treated and untreated nonwoven textile samples.

UNDERWATER DIAPHRAGM DISCHARGE, A NEW TECHNIQUE FOR POLYPROPYLENE TEXTILE SURFACE MODIFICATION

GABRIELA NEAGOE*[a], OLEKSANDR GALMIZ[a], ANTONÍN BRABLEC[a], JOZEF RÁHEĽ[a,b], ANNA ZÁHORANOVÁ[b]

[a] *Dep. of Physical Electronics, Faculty of Science, Masaryk University, Kotlářská 2, 611 37 Brno, Czech Republic,* [b] *Dep. of Experimental Physics, Comenius University, Mlynská dolina F2, 842 48 Bratislava, Slovak Republic*
gabriela.pirpiliu@yahoo.com

Keywords: underwater discharge, PP nonwoven, surface energy, contact angle

1. Introduction

Surface modification of textile materials extends over a wide range of alterations to provide desired single or multi-features for various applications. It is a highly focused area of research in which alterations to physical and/or chemical properties lead to new textile products that provide new applications or satisfy specific needs. These processes can involve numerous chemicals, some of which are toxic to humans and hazardous to the environment. In an effort to eliminate these harmful chemicals and waste products, surface modification and finishing via plasma treatment has become an attractive alternative.

Polypropylene (PP) is being increasingly used for industrial applications thanks to its beneficial properties and ability to be recycled. However, PP has a very low surface free energy, resulting in poor wettability and bonding strengths. To overcome this shortcoming, various techniques have been employed to modify the surface of polypropylene materials[1–3]. Plasma treatment is one of the most important surface modification techniques and has proven to be an environmentally friendly technique in the textile industry.

Plasma treatment of PP proceeds by a free-radical mechanism, which introduces a wide variety of oxidized functional groups onto the surface of the treated polymer. These oxidized functional groups may include C–OH, C=O, COOH, C–O–C, epoxy, ester, or hydroperoxide, and they are responsible for the changes in the polymer surface properties. The general effects of plasma treatment on the fiber surface are oxidation, generation of radicals, and etching.

During the last few years a lot of attention has been attracted by this field of underwater plasmas and its application in a variety of fields[4–8]. Important applications for these types of discharges had been restricted to the areas of water purification, sterilization, UV sources and shock wave generation.

Investigation of underwater discharges generated in water solutions at atmospheric pressure have shown effective production of OH radicals, solvated electrons and a number of others active species[8,9]. This primary source of radicals is often localised in a small region related to the size of the plasma discharge. Those radicals are highly reactive. Their oxidation potentials are one order of magnitude higher than usual chemical substances used to sterilise or to remove pollutants from the liquid phase.

Electrical breakdown in liquids is generally preceded by events called streamers. The two possible mechanisms for streamer initiation need to be considered: the first is due to electron avalanche which causes electrons to be injected in the liquid and drift to the cathode, and the other is due to the formation of micro-bubbles which cause gaseous cavities to be formed that give rise to electrical breakdown in the gas bubbles. The electric field around the electrode, or the streamer channel, is highly increased, which causes an intense field emission current that eventually vaporizes the water. Streamer discharge phenomena in water are known to be influenced by various factors, such as gap geometry, water conductivity, pulse duration and amplitude of the applied voltage[10].

2. Experimental setup

Distilled water was used as a working medium. The underwater plasma treatment was performed using two versions of experimental arrangement: single diaphragm (SD) discharge and double diaphragm (DD) discharge illustrated in Fig. 1. The detail of the discharge treating the textile is shown in Fig. 2.

The electrodes and the slit (diaphragm) were positioned under the water level. The electrodes were con-

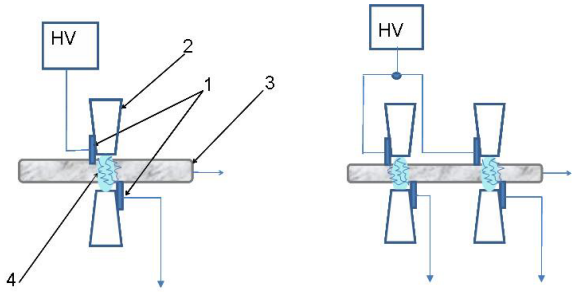

Fig. 1. **SD discharge (left) and DD discharge (right):** 1 – electrodes; 2 – diaphragm; 3 – polypropylene nonwoven fabric; 4 – discharge

Fig. 2. **Detail of the discharge**

nected to a pulsed HV power supply based on the double rotating spark gap. The maximum peak voltage reached a value of 40 kV DC and the maximum repetitive rate of pulses was 60 Hz.

Polypropylene nonwoven fabric of 50 gsm (grams per square meter) and 30 mm width was used for this experiment.

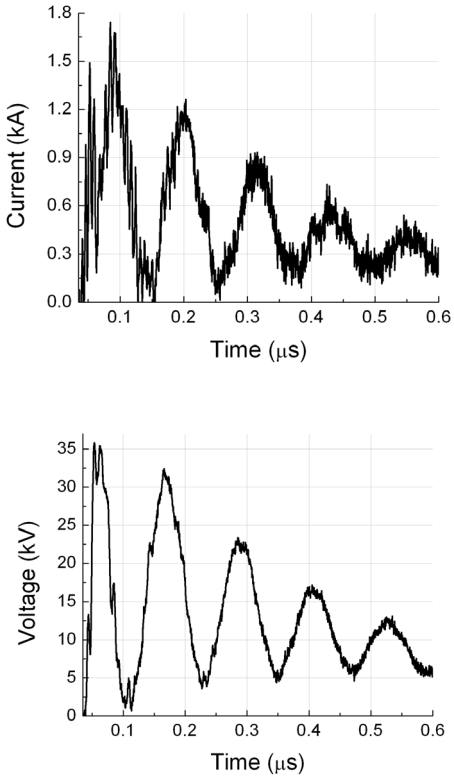

Fig. 3. **Waveforms of the discharge current and applied voltage pulses in distilled water**

The discharge was generated using a diaphragm electrode, where a narrow slits of 0.1×1×40 mm was positioned between two metallic electrodes at 2 cm mutual distance. The arrangement for double diaphragm is similar with the single diaphragm, but in this case we have two diaphragms in the same basin, the material undergoing two successive treatments. The distance between the diaphragms is 13 cm.

To keep optimal characteristics of the discharge the current and voltage measurements were done using the LeCroy WaveRunner 6100A (1GHz, 2GSa/s) Oscilloscope. Typical waveforms of the voltage and discharge current pulses are shown in Fig. 3.

We performed standard Optical Emission Spectroscopy (OES) to check the plasma discharge by means of the parameters[11]. The spectra profiles were measured by means of the Triax HR550 spectrometer, Jobin – Yvon (grating 1200 grooves, focal length 550 mm, CCD detector cooled by Peltier). The standard Griem's table (which takes into account the impact broadening by electron and quasi-static broadening by ions) of H_α line was used to determine electron temperature and density from H_α line profile[12]. The detailed description of the procedure is presented in (ref.[13]). Typical profile of H_α is shown in Fig. 4.

The total surface free energy (SFE) was determined from the measurements of the contact angles between the test liquids and the PP surfaces using a sessile drop technique. The system developed in our laboratory enables the observation of a solid–liquid meniscus directly by a CCD camera and the contact angles are determined from the CCD snapshots (Fig. 5); more information can be found in (ref.[14]).

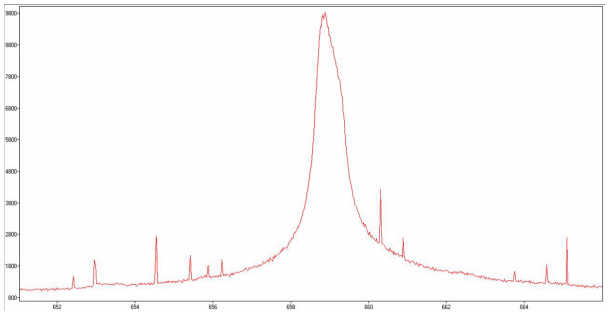

Fig. 4. **H_α line profile – original data, no filtering**

Fig. 5. **Snapshots of drops (diiodomethane) before (left) and after (right) treatment**

3. Results and discussion

The electron density changes from $1 \cdot 10^{22}$ m^{-3} to $2 \cdot 10^{24}$ m^{-3} while the electron temperature was practically constant $4 \cdot 10^4$ K in all experimental conditions studied. The error of the measured electron density was less than 5 %. The error of electron temperature was much higher, which is due to the weak dependence of the line profile on the electron temperature.

Given the nature of the plasma discharge (thin plasma filaments), the textile material is not uniformly treated in single diaphragm configuration. We noted that the wettability of the fabric was increased when the fabric was passing through two diaphragms. The second diaphragm proved to be an efficient tool for improving the wettability (Fig. 6) and not damage the fabrics. The optimum speed of PP through the diaphragms was 23 cm min^{-1} and the applied voltage was 25 kV.

The SFE (Kwok – Neumann model) of the untreated PP was 13.71 mJ m^{-2}. After double diaphragm treatment the SFE was increased to 31.51 mJ m^{-2}.

Contact angles between test liquids and polymers were measured in order to determine the total SFE using a sessile drop technique. Liquid drops on the plasma-activated polymer surface were imaged by the CCD camera and the contact angle was measured. The volume of each drop was 4 μl. Contact angles were measured for at least 10 drops for each liquid (Tab. I). The following six liquids were used: distilled water (H_2O), diiodomethane (CH_2I_2), formamide (CH_3NO), 1,2-ethanediol ($C_2H_6O_2$). Error of every measured angle is lower than 0.6°.

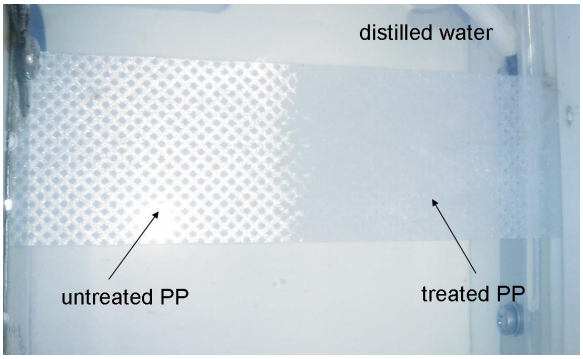

Fig. 6. **PP nonwoven treated by double diaphragm discharge (right) and untreated (left) immersed in distilled water**

Table I
Contact angles of liquids (in degrees) for untreated, single treated and double treated samples

Treatment type	H_2O	CH_2I_2	CH_3NO	$C_2H_6O_2$
untreated	110°	91°	107°	102°
SD	98°	70°	96°	78°
DD	89°	22°	53°	29°

The ageing of surface properties was also studied. The samples were stored in dry air and the SFE was measured during the time. The SFE did not change significantly during the time. The maximum decrease in the SFE was about 2 mJ m^{-2} after 14 days and afterwards the properties of the samples were stable.

4. Conclusion

It was found that the underwater diaphragm discharge (SD and DD configuration) can be used as possible application for surface modification of PP nonwoven. Double diaphragm discharge has increased the uniformity of the PP treatment.

It is shown that underwater diaphragm discharge treatment increases surface wettability of polypropylene nonwoven significantly. This is the result of an increase in surface free energy. Higher surface wetting is shown by a lower contact angle. Also, we observed that the ageing for 14 days has no significant effect on the surface free energy of the treated sample.

The results showed no thermal damage of PP after plasma treatment.

Surface modification by underwater plasma treatment has opened up new possibilities in relation to wettability and adsorption of nonwoven materials.

This research has been supported by the Czech Science Foundation under the contact numbers 202/09/2064 and 104/09/H080 as well as by the project CZ.1.05/2.1.00/03.0086 'R&D center for low-cost plasma and nanotechnology surface modifications' funded by European Regional Development Fund.

The work was also the result of the project implementation 26240220042 supported by the Research & Development Operational Programme funded by the ERDF.

REFERENCES

1. Slobodskoi S. A. et al.: Vopr. Technol. Ulavlivania i Pererab. Prod. Koksovania, *1978*, 71.
2. Sharma A. K., Locke B. R., Arce P., Finney W. C.: Hazard. Waste Hazard. Mater. *10*, 209 (1993).
3. Grimonpre D. R., Sharma A. K., Finney W. C., Locke B. R.: Chem. Eng. J. *82*, 189 (2001).
4. Monte M., De Baerdemaeker F., Leys C., Maximov A. I.: Czech J. Phys. *52*, Suppl. D, 724 (2002).
5. De Baerdemaeker F., Simek M., Clupek M., Lukes P., Leys C.: Czech J. Phys. *56*, Suppl. B, 1132 (2006).
6. Lukes P., Clupek M., Babicky V., Janda V., Sunka P.: J. Phys. D: Appl. Phys. *38*, 409 (2005).
7. Locke B. R., Sato M., Sunka P., Hoffmann M., Chang J.: Ind. Eng. Chem. Res. *45*, 882 (2006).
8. Sunka P., Babicky V., Clupek M., Lukes P., Simek Schmidt J., Cernak M.: Plasma Sources Sci. Technol.

8, 258 (1999).
9. Lukes P.: *Ph.D. Thesis*, Institute of Plasma Physics, Prague 2001.
10. Bruggeman P., Leys C., Vierendeels J.: J. Phys. D: Appl. Phys. *40*, 1937 (2007).
11. Bruggeman P., Verreycken T., Gonzalez M. A., Walsh J. L., Kong M. G., Leys C., Schram D. C.: J. Phys. D: Appl. Phys. *43*, 124005 (2010).
12. Griem H. R.: *Spectral line broadening by plasma*. Academic Press, New York 1974.
13. Brablec A., Slavíček P., Sťahel P., Čižmár T., Trunec D., Šimor M., Černák M.: Czech. J. Phys. *52*, Suppl. D 491 (2002).
14. http://www.advex-instruments.cz/

G. Neagoe[a], O. Galmiz[a], A. Brablec[a], J. Ráhel[a,b], and A. Záhoranová[b] *([a] Dep. of Physical Electronics, Faculty of Science, Masaryk University, Brno, Czech Republic; [b] Dep. of Experimental Physics, Comenius University, Bratislava, Slovak Republic):* **Underwater Diaphragm Discharge, a new Technique for Polypropylene Textile Surface Modification**

Underwater single and double diaphragm discharge were used for surface modification of polypropylene nonwoven. The discharge was generated in distilled water. Optical Emission Spectroscopy (OES) was used to determine temperature and density of the plasma electrons. The total surface free energy (SFE) was determined from the measurements of the contact angles. It was found that the double diaphragm arrangement improved the uniformity and wettability of PP treatment.

Chem. Listy *106*, s1475−s1481 (2012) CEPLANT

STEEL SURFACE TREATMENT AND FOLLOWING AGING EFFECT AFTER COPLANAR BARRIER DISCHARGE PLASMA IN AIR, NITROGEN AND OXYGEN

VADYM PRYSIAZHNYI[a,*], JINDŘICH MATOUŠEK[b], MIRKO ČERNÁK[c]

[a] *Faculty of Science, Masaryk University, Kotlarska 2, 611 37 Brno, Czech Republic,* [b] *Department of Physics, Faculty of Science, J. E. Purkinje University, Ceske mladeze 8, 400 96 Usti nad Labem, Czech Republic,* [c] *Faculty of Mathematics, Physics and Informatics, Comenius University, Mlynská dolina, 842 48 Bratislava, Slovak Republic*
mr.vodik@gmail.com

Keywords: steel surface; air plasma treatment; DCSBD; aging effect; hydrophobic recovery.

1. Introduction

Non-thermal atmospheric plasma surface processing is a hot topic for applied research nowadays. Despite all the complications to fully understand the plasma chemistry, it is already used in many industrial applications. Main reasons are its benefits, such as environmentally friendly technology, low cost of maintenance, and easy implementation of plasma in production lines (compared with low-pressure plasma treatments). Due to the wide range of possibilities to change plasma chemistry (by adding gas mixtures, changing electrode geometry or discharge type), it attracts more attention for applications without high requirements for treatment on nanosize level, like adhesion improvement, increase quality of painting for automotive, construction or aerospace industries. Surface pre-treatment of steel for these kinds of applications is often required. From the variety of surface modifications of steel we are particularly interested in low-cost surface pre-treatment for painting/adhesion enhancement. Different pre-treatment methods were developed for surface modifications, such as sol-gel[1], electrochemical[2], laser[3] or surface coating by adhesive layer (e.g. chromization[4]).

Different plasma sources and approaches were used to study the effects of plasma pre-treatment of steel surface. Low-pressure plasma treatment for metal surface modifications was studied first[5]. It was typically used to implant additives in surface to modify material (nitriding of steel[6]) or to deposit a coating onto the surface (low-pressure polymerization[7]). Nowadays low-pressure treatment of steel is not considered for large scale metal industry because of its high maintenance costs.

Several atmospheric pressure plasma sources have been developed for surface modifications[8–10]. Plasma treatments using cheap gases (like air, nitrogen, argon or oxygen) are at high interest as they are economically beneficial[11]. The use of plasma jet systems for metal surface treatments was reported in several works[12,13]. For flat surface treatments the use of plasma jet has more complications, like insufficient homogeneity or long treatment duration.

Dielectric Barrier Discharge (DBD) plasma sources are proven to be efficient for flat surface pre-treatments[14]. There are many examples when DBD plasmas are used in surface treatment of textiles, plastics, wood and metals. An important issue of plasma pre-treatment, when no coating is deposited while plasma is in contact with surface, is its non-permanent character or so-called aging effect.

The typical parameter that can evaluate pre-treatment efficiency is surface wettability or its quantitative parameter, the surface free energy (SFE). In most cases the surface free energy is increasing as a result of the surface pre-treatments using atmospheric pressure plasmas[15]. Aging effect (or hydrophobic recovery) can be defined as a decrease of the SFE to lower values (not always original value before plasma treatment) after several hours or days[16]. As a consequence, the aging effect may play important role when a time delay between technological steps is necessary. The detailed study of aging effect was done for polymer surfaces, where it is an important technological issue[17,18]. But even though the presence of aging effect after plasma treatment of metal substrates was shown[19,20], this topic is still not clear enough.

Air humidity is another important parameter, which needs to be taken into account when ambient air plasma treatments are considered. When non-thermal (cold) plasmas at atmospheric pressure are used for the surface treatments, the humidity affects the chemical reactions in plasma volume[21]. The effect of humidity on plasma parameters for dielectric barrier discharges (DBDs) was studied and generation of $-NO_x$ radicals in plasma volume was measured and modeled theoretically[22,23]. However, we are not aware of any results explaining in more details the effect of humidity on the plasma treatment of steel.

This work describes the characteristics of common low-carbon steel after surface DBD plasma treatments, the increase of wettability after the plasma treatments and the explanation of the following aging effect of plasma treated steel surfaces. Plasma treatments were done using the Diffuse Coplanar Surface Barrier Discharge (DCSBD), which generates surface barrier discharge plasma with higher power density that conventional volume DBD plasma sources.

A detailed study of aging effect, i.e. decrease of the surface free energy while storing the plasma treated surfaces, and influence of humidity was performed by the surface free energy and X-ray photoelectron spectroscopy techniques.

2. Experimental

Steel samples were cut from steel sheets (1.0330 steel; 1 mm thick; Fe – max. 99.19 %, C – max. 0.12 %, P – max. 0.045 %, S – max. 0.045 %, Mn – max. 0.6 %). After cutting (for the surface free energy the samples had size 10 cm × 3 cm, for the X-ray photoelectron spectroscopy samples had size 1 cm × 1 cm), a two steps cleaning process was performed for all the samples. During the first step, chemical degreasing using dust-free tissue was done to remove metal dust particles or leftovers of grease. In the second step, the samples were cleaned in ultrasonic bath for 5 minutes in isopropanol; cleaned in ultrasonic bath for 5 minutes in acetone. Subsequently the samples were dried with flow of compressed air and stored at least one day in laboratory air before plasma treatments.

The Diffuse Coplanar Surface Barrier Discharge (DCSBD) source was used for steel surface treatments[24]. This plasma source is a type of surface barrier discharge. It allows generating highly non-equilibrium high-power density plasma in form of a thin planar layer with thickness of about 0.3−0.5 mm as it is shown in Fig. 1a. The coplanar electrodes were produced on the alumina ceramics that have size 26 cm × 9.3 cm. Silver metal electrodes were evaporated on the bottom side in etched channels 1.5 mm wide, with 1 mm distance in between them. The plasma was generated on 20 cm × 8 cm area, where thirty eight metal stripes were produced, as it is shown in Fig. 1b.

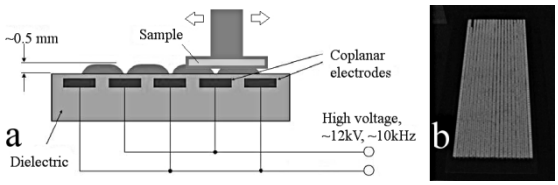

Fig. 1. **(a) Schema of DCSBD plasma source and (b) image of the discharge running in ambient air with exposition time 1/1000 s**

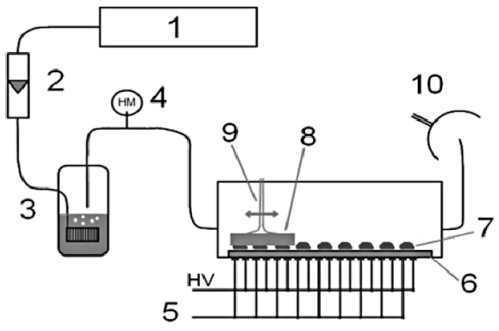

Fig. 2. **Schema of experimental setup.** 1 – air compressor, 2 – gas flow meter, 3 – bubbler, 4 – humidity meter, 5 – high voltage, 6 – Al_2O_3 ceramic, 7 – plasma layer, 8 – sample, 9 – movable sample holder, 10 – gas exhaust

Table I
Surface tension (σ_l) and its polar (σ_l^{polar}) and dispersive (σ_l^{disp}) part for test liquids used

	σ_l	σ_l^{polar}	σ_l^{disp}
Distilled water	72.6	21.6	51
DMSO	44	36	8
50% K_2CO_3 in water	103.8	34	69.8

The plasma surface modifications were performed at room temperature by moving the sample above the DCSBD electrode system with a constant speed. Dry, ambient and humid air, nitrogen and oxygen were used as a plasma gas. The humidity of air was set from less than 2 % RH to more than 90 % RH. The plasma treatment time was 5 s, 40 s and 100 s.

The distance between the sample and the DCSBD electrode was set to 0.35 mm. The applied power, which was measured by Energy Check 3000 from Voltcraft, was set to 340 W. This value corresponds to the power density of 1.9 W cm^{-2}. A schema of the experimental setup is shown in Fig. 2.

The wettability was estimated by measuring the surface free energy (SFE) of steel surface using sessile-drop method. The SFE measurements were performed by a Surface Energy Evaluation System (supplied from Advex Instruments, Czech Republic). This method requires to measure values of contact angles using a few test liquids with well-defined properties. For current measurements the volume of each drop was 2 μl and the average value of at least 6 droplets was calculated for each test liquid and for each sample. Distilled water, dimethyl sulfoxide (DMSO) and 50 % solution of K_2CO_3 in deionized water were used as test liquids. The total surface tension and its polar and dispersive parts for the different liquids are presented in Table I (ref.[25,26]). The Owens-Wendt regression model was used to calculate the surface free energy using measured values of contact angles[27].

The X-ray photoelectron spectroscopy (XPS) measurements were done to evaluate the changes in chemical composition and bond structure occurred on the steel surface after plasma treatments. The XPS measurements were performed using a spectrometer equipped with a hemispherical analyzer operated in FAT mode (Phoibos 100 from company Specs). The Al K_{alpha} X-ray source (1486.7 eV) was operated at 200 W. The survey spectra were recorded at pass energy 40 eV with an energy step of 0.5 eV, while the high-resolution XPS spectra at pass energy 10 eV with an energy step of 0.05 eV. All spectra were referenced to the peak of aliphatic C-C bond at 285 eV. A Shirley-type background was subtracted from all spectra prior to data processing. Binding energies and peak fitting routines were performed by CasaXPS software.

3. Results and discussion

3.1. Surface wettability

The results of the SFE measurements showed the significant increase of the surface free energy of treated steel surfaces compared to the untreated ones. One of the reasons for the increased wettability can be the change of the surface roughness. However, the results of AFM measurements that were done on the steel substrates didn't show changes in the surface morphology and estimated surface roughness was not altered after the plasma treatment (the peak-to-peak values of the steel surface substrates was approximately 2 μm on the areas without visible scratches for both untreated and treated samples). Therefore, the observed changes in the surface wettability are related to the changes in surface composition/surface chemical structure.

As an example, the increase of the surface free energy as a function of treatment duration in ambient air is shown in Fig. 3. In this and further figures with SFE measurements the total height of the bar stands for the value of the surface free energy (white part of bar corresponds to its dispersive component and grey part of bar corresponds to the polar component). The increase of the SFE is due to the increase of its polar component, as shown in Fig. 3. For such cases a generation of polar functional groups on the surface can be expected. Taking into account that the treatment was done in air, these functional groups might be the OH ones.

Aging effect of plasma treated steel surfaces was measured up to 7 days after the plasma treatments, showing a decrease of the surface wettability while storage. The results of the SFE measurements (plasma treatment time 40 s) in air after 1, 2, 3, 4 and 7 days of storage in ambient air are shown in Fig. 4. The hydrophobic recovery of the plasma treated steel surfaces was reaching the saturation after about 2 days of storage. The changes in ratio between polar and dispersive component immediately after the plasma treatment and after storage in air for two days for different plasma durations are presented in Fig. 5. Note the different character of aged surfaces treated in dry (Fig. 5a) and wet air (Fig. 5b). Polar component changes with increasing of the treatment time in an inverse way. In dry air, for longer treatment duration the polar component of the SFE was decreasing. In wet air, the value of polar component was growing for higher treatment durations. Proposed assumption about generated OH groups allows explaining measured data. Higher number of OH groups is conserved on the surface for the samples stored in wet air, because of water vapors presented in wet air. Also higher number of polar groups will remain on the surface after longer treatment, because higher number of groups was generated on steel surface by plasma. Smaller number of OH groups was conserved on the surface during storage in dry air.

To examine the aging effect, additional series of measurements were done for treated steel samples in ambient air, nitrogen and oxygen. After treatment the samples were stored in ambient air and vacuum. To ensure the aging process is finished it was decided to store samples for 4 days (see Fig. 4). The samples were stored in ambient air at room temperature with humidity ~40 % RH. Vacuum storage was done in the oil-free vacuum chamber with pressure about 10^{-3} Pa.

The results of these measurements are presented in Fig. 6, Fig. 7 and Fig. 8 for plasma treatment in air, nitrogen and oxygen, respectively. The following observations were found after these measurements.

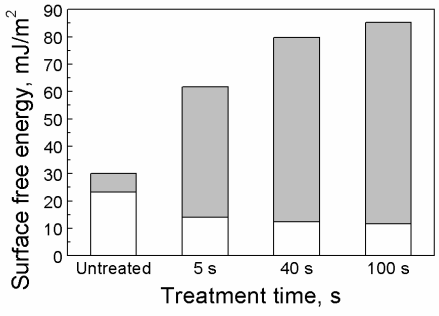

Fig. 3. **Change of the SFE for steel sheets (total bar height) after the air DCSBD plasma treatment.** Treatment conditions: ambient air, 40 s

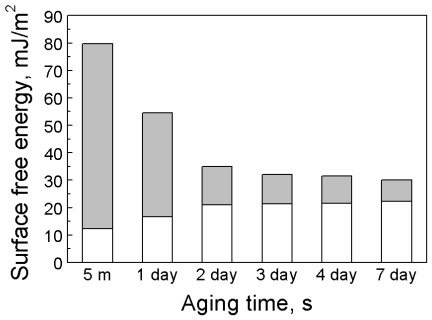

Fig. 4. **Aging effect of plasma treated steel sheets depending on a storage time in laboratory air.** Treatment conditions: ambient air, 40 s

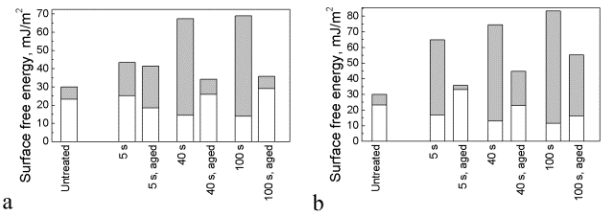

Fig. 5. **Changes in SFE depending on a treatment gas, treatment time and aging conditions. (a) plasma treatment in dry air, (b) plasma treatment in wet air.** Aging done in ambient air for 2 days

1) The values of the SFE are in the same range of 65–70 mJ m^{-2} for 5 s plasma treatments and 76–82 mJ m^{-2} for 40 s treatments.

2) The proportion of polar-to-dispersive component of the SFE measured on the plasma treated steel surfaces after the treatment in all gases are roughly the same.

3) The treatment in air and oxygen gave similar results, while the measurements on the samples treated in nitrogen show higher value of dispersive component for short treatment times of 5 s.

4) Based on the obtained data it can be assumed that the most important impact on the surface wettability has the post-treatment surface reactions.

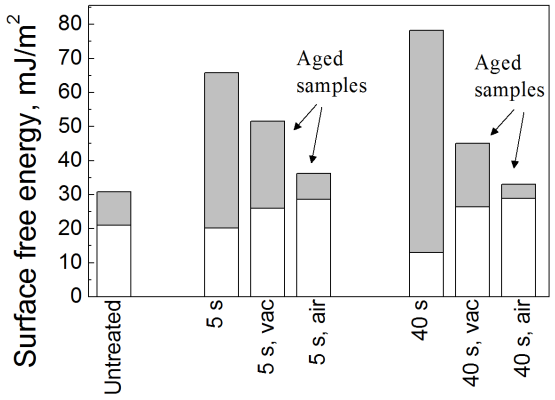

Fig. 6. **Changes of the SFE after air DCSBD treatment of steel surfaces with subsequent aging for 4 days in ambient air and vacuum**

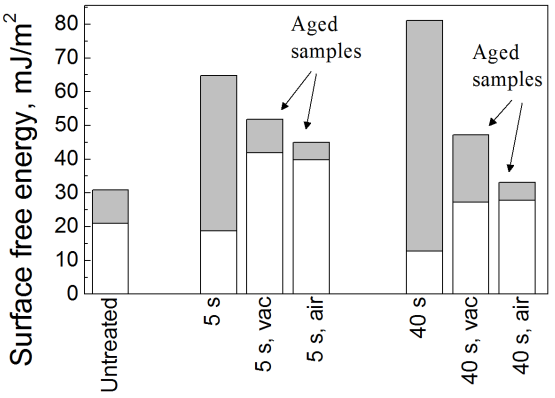

Fig. 7. **Changes of the SFE after nitrogen DCSBD treatment of steel surfaces with subsequent aging for 4 days in ambient air and vacuum**

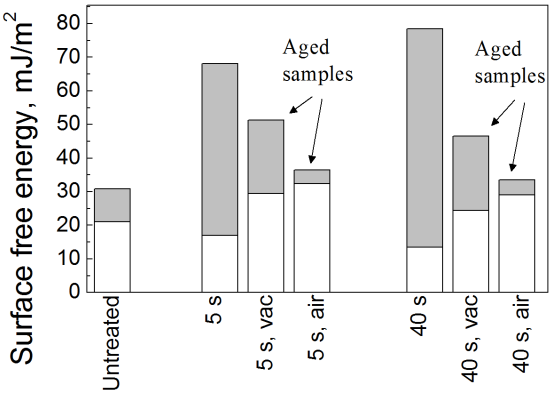

Fig. 8. **Changes of the SFE after oxygen DCSBD treatment of steel surfaces with subsequent aging for 4 days in ambient air and vacuum**

3.2. Surface chemical composition and bond structure

In our previous study[28] it was shown that more than 10 s treatment times is needed to obtain homogeneous treatment on aluminium. Therefore, most of the samples measured by the XPS technique were treated for 40 s. The surface composition depending on treatment conditions are presented in Tab. II. Note that the increase of iron and oxygen concentration is mostly due to reduction of carbon content after the plasma treatment.

As expected, the content of atomic iron was lowest for oxygen plasma treatment (highest oxidation is expected), followed by the air and nitrogen treatments.

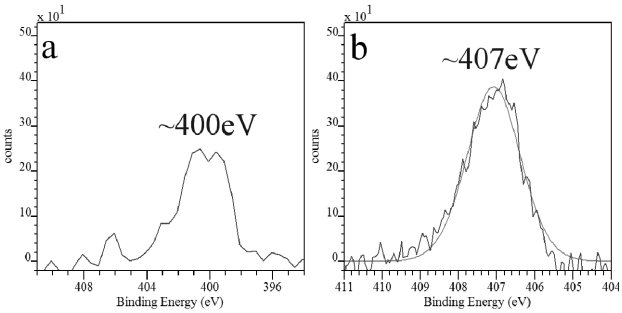

Fig. 9. **High-resolution N 1s peak on steel surface: a) weakly bonded nitrogen, plasma treatment in nitrogen for 40 s; b) nitrate group, plasma treatment in ambient air for 40 s**

Table II
Surface composition of steel samples after plasma treatment in various gases for 40 s

	Fe [at%]	O [at%]	C [at%]	N [at%]	Mn [at%]
Untreated	7	42	49	–	1
Dry air	16	63	16	3[a]	2
Ambient air	16	61	15	6[a]	4
Wet air	16	60	13	10[a]	1
Oxygen	10	60	25	2[b]	3
Nitrogen	22	61	11	2[b]	4

[a] Nitrate group, [b] weakly bonded nitrogen due to presence of residual air

The presence of N 1s peak in the XPS spectra measured on the plasma treated steel surfaces was evidenced. The content of atomic nitrogen was proportional to air humidity (see Tab. II). N 1s peak had two subcomponents at binding energies 400 eV and 407 eV. The first one (Fig. 9a) is corresponding to weakly bonded nitrogen[29] and was found on the steel substrate after nitrogen and oxygen plasma treatment. Most probably its presence is due to residual air of the plasma reactor. The second component (Fig. 9b) is corresponding to the nitrate ($–NO_x$) group. It was identified by the shift of binding energy[30] of the N1s peak to the value of 407 eV. The results allow us to assume that $–NO_x$ functional groups were generated on the steel surface during the humid air plasma treatment, which is in a good agreement with literature about air DBD plasma chemistry[31], where nitrate radicals are one of the intermediate products of complex series of chemical reactions.

The XPS measurements were performed on aged samples to determine the role of aging environment. The samples treated in ambient air, nitrogen and oxygen were stored for 4 days in (i) oil-free vacuum chamber, where the pressure was not exceeding $2 \cdot 10^{-5}$ Pa and (ii) ambient air. The changes in atomic composition after storage are shown in Table III, Table IV and Table V for DCSBD plasma treatments in ambient air, nitrogen and oxygen, respectively. The following observations were established:

1) Decrease of carbon content was measured for longer plasma treatment duration for treatments in air, nitrogen and oxygen. This proves the plasma treatment has the cleaning effect. Unlike for polymer surfaces, longer treatment duration is needed to obtain the cleaning effect after the DBD plasma (i.e. higher energy impact to unit surface). For instance, polymer surface oxidation can be achieved in fractions of a second.

2) Aging in air is leading to the highest re-adsorption rates of airborne hydrocarbon contaminants, while the situation is opposite for plasma treated samples after storage in vacuum.

3) The nitrate groups created after the plasma treatment in ambient air remain on the surface after storage in vacuum.

Table III
Surface composition of plasma treated steel in air and aged in different conditions for 4 days

	Fe [at%]	C [at%]	O [at%]	N [at%]	Mn [at%]
Untreated	7	49	42	–	1
5 s	9	23	58	5[a]	5
40 s	16	15	61	6[a]	3
aged, air	17	21	57	–	5
aged, vacuum	12	19	61	3[a]	5

[a] Nitrate group

Table IV
Surface composition of plasma treated steel in nitrogen and aged in different conditions for 4 days

	Fe [at%]	C [at%]	O [at%]	N [at%]	Mn [at%]
Untreated	7	49	42	–	1
5 s, N_2	15	27	54	2[b]	3
40 s, N_2	22	11	61	2[b]	4
aged, air	18	18	60	1[b]	3
aged, vacuum	22	16	59	1[b]	2

[b] Weakly bonded nitrogen due to presence of residual air

Table V
Surface composition of plasma treated steel in oxygen and aged in different conditions for 4 days

	Fe [at%]	C [at%]	O [at%]	N [at%]	Mn [at%]
Untreated	7	49	42	–	1
5 s, O_2	12	22	62	2[b]	2
40 s, O_2	10	22	63	2[b]	3
aged, air	21	18	59	–	3
aged, vacuum	12	21	63	2[b]	3

[b] Weakly bonded nitrogen due to presence of residual air

Table VI
Assignment of the Fe $2p_{3/2}$ peak components

Component	Binding energy [eV]	FWHM [eV]
Fe	707.0	2.0
FeO	709.6	2.2
FeOOH	711.8	3.4
Fe_2O_3	710.8	2.4

In order to study the changes in the bond structure, the high resolution Fe $2p_{3/2}$ peak was fitted by 4 components according to literature[32] (the Fe $2p_{3/2}$ spectra are not shown here). Component at 707.0 eV can be attributed to Fe in metallic state. This component decreased after all types of treatments while the increase of the oxygen containing groups bonded to Fe was observed after the plasma treatment.

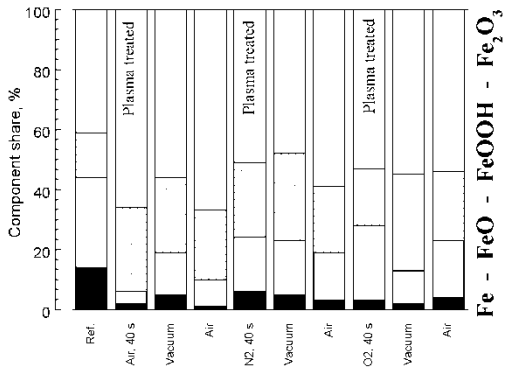

Fig. 10. **Ratio for Fe $2p_{3/2}$ components depending on plasma gas atmosphere and following aging in different environments after 4 days of storage**

The Fe $2p_{3/2}$ components and the probable chemical species related to them are listed in Tab. VI. Overall results for different treatment atmospheres and aging conditions are presented in Fig. 10. The x-axis should be understood as follows: "Ref." means untreated sample, bars marked "Plasma treated" represents the ratio of iron components after the plasma treatment, bars with mark "Vacuum" and "Air" represent the ratio of iron components for samples stored for 4 days in vacuum and air, respectively.

The increase of oxide (Fe_2O_3) and hydroxide (FeOOH) content after plasma treatment was observed for all treatment conditions. Also, independent on carbon content, the amount of atomic iron is lower for plasma treated samples. No obvious regularities between amount of FeOOH and surface wettability were found as opposed to plasma treated aluminium surfaces[33]. The increase of hydroxide component, though, shows that the assumption of generated OH groups was correct, but reduced wettability is due to hydrocarbon re-adsorption.

4. Conclusions

The effects of plasma gas (including air humidity) and aging environment on the coplanar barrier discharge plasma treatment of low-carbon steel surface was reported. The plasma treatment was done using the Diffuse Coplanar Surface Barrier Discharge (DCSBD) and resulted in significant increase of the surface free energy. For the typical plasma treatment conditions the surface free energy was growing from 29 mJ m^{-2} to over 75 mJ m^{-2}.

The aging effect of the plasma treatment was measured for storage in air and vacuum. The obtained results from the SFE measurements were explained using the results of XPS technique. It is apparent that plasma treatment leads to surface cleaning from hydrocarbon contaminants and generation of hydroxyl, nitrate and iron oxide. Changes in wettability can't be explained only by relative quantities of atomic carbon or iron hydroxides on the steel surface. Based on the measured results it is reasonable to suppose that both contaminants and ratio between oxide/ hydroxide components defines the surface wettability of steel. Generation of $-NO_x$ groups on steel surface after plasma treatment in humid air was shown. The nitrate surface groups are not stable in air and their stability is higher in vacuum.

This research has been supported by the project CZ.1.05/2.1.00/03.0086 'R&D center for low-cost plasma and nanotechnology surface modifications' funded by European Regional Development Fund, by the Grant Agency of the Academy of Sciences of the Czech Republic under contract KAN311610701 and by the Czech Science Foundation (Projects No. 104/08/0229 and 202/09/2064).

REFERENCES

1. Metroke T. L., Parkhill R. L., Knobbe E. T.: Prog. Org. Coat. *41*, 233 (2001).
2. Jegannathan S., Sankara Narayanan T. S. N., Ravichandran K., Rajeswari S.: Surf. Coat. Technol. *200*, 4117 (2006).
3. Pereira A., Cros A., Delaporte P., Marine W., Sentis M.: Appl. Surf. Sci. *208–209*, 417 (2003).
4. Wang Z. B., Lu J., Lu K.: Acta Mater. *53*, 2081 (2005).
5. Sapieha S., Cerny J., Klemberg-Sapieha J. E., Martinu L.: J. Adhesion *42*, 91 (1993).
6. Liang W.: Appl. Surf. Sci. *211*, 308 (2003).
7. Yasuda H., Matsuzawa Y.: Plasma Process. Polym. *2*, 507 (2005).
8. Plasma Treat Open Air. http://www.plasmatreat.com/plasma-technology/openair-atmospheric-plasma-technique.html (7.12.2012).
9. PlasmaSpot. http://www.vitoplasma.com/en/30 (7.12.2012).
10. Corotec Corporation. http://corotec.com/products/plasmajet-specs.html (7.12.2012).
11. Roth J. R.: *Industrial Plasma Engineering: Principles*. Taylor & Francis, University of Tennessee, Knoxville, USA, 1995.
12. Kim M. C., Song D. K., Shin H. S., Baeg S.-H., Kim G. S., Boo J.-H., Han J. G., Yang S. H.: Surf. Coat. Technol. *171*, 312 (2003).
13. Tang S., Kwon O.-J., Lu N., Choi H.-S.: Surf. Coat. Technol. *195*, 298 (2005).
14. Goossens O., Dekempeneer E., Vangeneugden D., Van de Leest R., Leys C.: Surf. Coat. Technol. *142–144*, 474 (2001).
15. Mantel M., Wightman J. P.: Surf. Interface Anal. *21*, 595 (1994).
16. Roth J. R., Chen Z. Y.: Acta Metal. Sin. *14*, 391 (2001).
17. Morent R., De Geyter N., Leys C., Gengembre L., Payen E.: Surf. Coat. Technol. *201*, 7847 (2007).
18. O'Connell C., Sherlock R., Ball M. D., Aszalos-Kiss

B., Prendergast U., Glynn T. J.: Appl. Surf. Sci. *255*, 4405 (2009).
19. Kim M. C., Yang S. H., Boo J.-H., Han J. G.: Surf. Coat. Technol. *174–175*, 839 (2003).
20. Shin D. H., Bang C. U., Kim J. H., Hong Y. C., Uhm H. S., Park D. K., Kim K. H.: IEEE Trans. Plasma Sci. *34*, 1241 (2006).
21. Benstaali B., Boubert P., Cheron B. G., Addou A., Brisset J. L.: Plasma Chem. Plasma Process. *22*, 553 (2002).
22. Tochikubo F., Uchida S., Yasui H., Sato K.: Jpn. J. Appl. Phys. *48*, 076507 (2009).
23. Iskenderova K., Chirokov A., Gutsol A., Fridman A., Kennedy L., Sieber K. D., Grace J. M., Robinson K. S.: *15th International Symposium on Plasma Chemistry, Orléans, France, 9–13 July 2001*. Symposium Proceedings II, 443.
24. Černák M., Černáková L'., Hudec I., Kováčik D., Zahoranová A.: Eur. Phys. J. Appl. Phys. *47*, 22806 (2009).
25. Kwok D. Y., Neumann A. W.: Adv. Colloid Interface Sci. *81*, 167 (1999).
26. *Potassium Carbonate Handbook, Technical Data for Potassium Carbonate*, Armand Products, Table 10, www.armandproducts.com/pdfs/k2so3P33_46.pdf.
27. Rudawska A., Jacniacka E.: Int. J. Adhes. Adhes. *29*, 451 (2009).
28. Prysiazhnyi V., Vasina P., Panyala N. R., Havel J., Cernak M.: Surf. Coat. Technol. *206*, 3011 (2012).
29. Gredelj S., Gerson A. R., Kumaring S., Cavallaro G. P.: Appl. Surf. Sci. *174*, 240 (2001).
30. *NIST X-ray Photoelectron Spectroscopy Database*, *Version 3.5*. National Institute of Standards and Technology, Gaithersburg, 2003, http://srdata.nist.gov/xps/.
31. Herron J. T., Green D. S.: Plasma Chem. Plasma Process. *21*, 459 (2001).
32. Yamashita T., Hayes P.: Appl. Surf. Sci. *254*, 2441 (2008).
33. Prysiazhnyi V., Zaporojchenko V., Kersten H., Černák M.: Appl. Surf. Sci. *258*, 5467 (2012).

V. Prysiazhny[a], J. Matoušek[b], and M. Černák[c]
([a] Faculty of Science, Masaryk University, Brno, Czech Republic, [b] Department of Physics, Faculty of Science, J. E. Purkinje University, Usti nad Labem, Czech Republic, [c] Faculty of Mathematics, Physics and Informatics, Comenius University, Bratislava, Slovak Republic): **Steel Surface Treatment and Following Aging Effect after Coplanar Barrier Discharge Plasma in Air, Nitrogen and Oxygen**

The results on plasma treatment of low-carbon steel sheets by Diffuse Coplanar Surface Barrier Discharge are reported. Significant increase of the surface free energy from 29 mJ m^{-2} to over 75 mJ m^{-2} after the plasma treatment was observed. A detailed X-ray photoelectron spectroscopy study was performed to understand the reasons for increased wettability as well as following hydrophobic recovery. Based on the obtained results it was found that the aging effect is related to the transformation in the bond structure between Fe, O and OH and re-adsorption of hydrocarbon contaminants from air. The presence of surface nitrate groups was measured after the treatments in humid air plasma as well.

MODELLING OF REACTIVE MAGNETRON SPUTTERING WITH FOCUS ON CHANGES IN TARGET UTILIZATION

TEREZA SCHMIDTOVÁ*, PETR VAŠINA

Deartment of Physical Electronics, Faculty of Science, Masaryk University, Kotlářská 2, 611 37 Brno, Czech Republic
dorain@physics.muni.cz

Keywords: reactive magnetron sputtering, modelling, target utilization

1. Introduction

The deposition of thin films by reactive magnetron sputtering is frequently used in many industrial applications. For growing of oxides or nitride thin films reactive gases are commonly added to the deposition chamber. To set the desired experimental conditions for the deposition process, it is natural to adjust the reactive gas flow rather than the partial pressure of the reactive gas. It is simpler and easier to perform, however, the process controlled by the supply flow of the reactive gas exhibits undesirable hysteresis behaviour.

The reactive gas added to the deposition chamber causes the forming of the compound molecules on the target surface which are being removed by the sputtering. The local composition of the target results from the balance between the creation and the destruction of the compound molecules. These processes are sometimes in a simplified way referred to as the target poisoning and the target cleaning. The origin of the hysteresis behaviour lies in the difference in the sputtering yield of metal atom from the clean and from the compound part of the cathode surface[1]. If the reactive gas supply flow is low, the resulting fraction of the compound molecules on the target surface is low, too. The process runs in the so-called metallic mode. If the reactive gas supply flow is increased up to a certain value, the newly generated conditions force the partial pressure of the reactive gas to increase often very dramatically. The process conditions are changed and the transition from the metallic to the compound mode occurs[2–4]. In order to acquire the reverse decrease of the partial pressure of the reactive gas it is necessary to substantially decrease the reactive gas supply flow.

In the magnetron configuration, the presence of the magnetic field causes a formation of a high density plasma in a shape of a toroid in front of the magnetron target and thus the sputtering of the target is very non-uniform[5–8]. Although it would be highly desirable to utilize the target material completely, due to the non-uniformity of the discharge current density, it is infeasible. The scale coefficient of the target usage by sputtering is a factor of the target utilization. The target utilization is a relative quantity proportional to the amount of the target material that is sputtered under certain conditions during the deposition. In practic, the target utilization is determined by the relative change in the weight of the target after it becomes depleted at the racetrack part of the target by sputtering. Nowadays, target manufacturers can reshape the targets to increase the target utilization simply by adding more material to the racetrack area.

In the case of the sputtering in the non-reactive atmosphere, the target erosion profile copies the profile of the discharge current density over the target area. Therefore, also by reshaping of the magnetic field structure over the target a higher target utilization can be achieved. At present, a wide range of magnetic field configurations exits on the market. Standard configurations are two pole magnetics with the target utilization approximately 30 %, but above standard multi pole magnetics that deform and flatten the structure of the magnetic field over the target area that gives the target utilization approximately 60 % can be found. By an increase of the target utilization, the cost of the target material for deposition of the thin film can be reduced. In the case of precious metals a considerable saving can be made.

If a reactive gas is added into the sputtering process, the conditions in the whole deposition chamber including the target surface change. Simultaneous poisoning and cleaning of the target causes the compound fraction in the target parts with lower discharge current density to be higher than in the racetrack part which is sputtered more intensively. The target composition is becoming non-uniform and due to the difference between sputtering yields of the metal atoms from the clean parts of the target and from the parts covered by the compound, the sputtering rate of the target is changing, too. It can be expected that the target utilization at different conditions during the reactive sputtering deposition process can be at least slightly reduced compared to the situation without any presence of the reactive gas. The goal of this paper is to predict the scale of these changes in the target utilization during the evolution of the reactive sputtering deposition process. Particularly, the role of the profile of the discharge current density on the changes of the target utilization during the reactive magnetron sputtering is studied.

2. Model specifications

The reactive magnetron sputtering process is usually simulated by models based on the well known Berg model[9–11] which is a parametric model describing the behaviour of the sputtering process. It has been used to state

very interesting predictions and to explain some non-trivial observations. Just to mention the most recent research; for example it states that the hysteresis can be reduced or even eliminated not only by an increase of the pumping speed[12–14] but also by a reduction of the target erosion zone[15], the model was also used to predict the temporal evolution of reactive magnetron sputtering[16], etc. The original Berg model and its successors assume the uniform discharge current density and consequently, they cannot predict the target utilization. Assuming the uniform discharge current density, the target utilization is always independent of the experimental conditions. Recently, we intentionally extended on Berg model in order to accommodate the non-uniform discharge current density[17]. Therefore it allows the investigation of the reactive sputtering of targets exposed to different discharge current density profiles at different process conditions. For purposes of this paper two Gaussian profiles of the discharge current density are closely studied (see Fig. 1). Both show the maximum value at the half radius of the target and values of FWHM are 0.02 m and 0.04 m, which correspond to the target utilization in pure metallic mode (i.e. without any presence of the reactive gas in the deposition chamber) of 30 % and 60 %, respectively.

The process conditions that are studied in details are represented by the points of interest during the evolution of the sputtering process, see Fig. 2. Point A is the situation without any reactive gas and it is denoted as the pure metallic mode, point B is set at 1 sccm of the reactive gas to represent the metallic mode, the moment just before the transition between metallic and compound mode (M-C transition) corresponds to point C, point D is the situation just after the metallic to compound mode transition and point E is chosen at 4.5 sccm of the reactive gas to represent the compound mode. Note that points A, B and E are fixed on the flow of the reactive gas but points C and D are

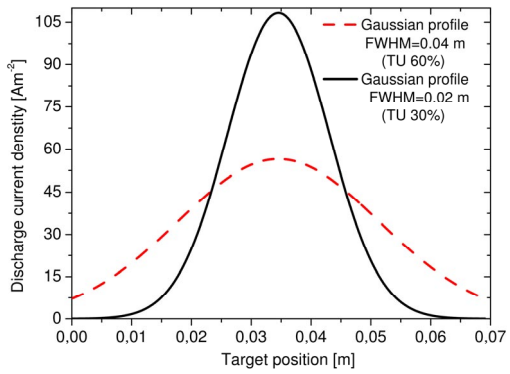

Fig. 1. **Two Gaussian profiles of the discharge current density over the target radius.** The maximum is placed at half radius of the target and the FWHMs are 0.02 m and 0.04 m. Corresponding target utilizations in pure metallic mode are 30 % and 60 %, respectively

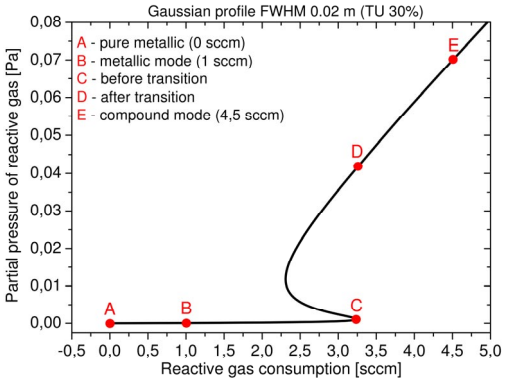

Fig. 2. **Declaration of the points of interests in the plot of the partial pressure of the reactive gas as a function of the reactive gas supply flow for the profile with FWHM = 0.02 m**

variable depending on the moment of the transition, which occurs for the different profiles of the discharge current density at different reactive gas supplies.

3. Results and discussion

3.1. Modelling of the lateral target composition

Modelled lateral variations of the compound fraction at the target for two studied Gaussian discharge current density profiles are shown in Fig. 3. The edges of the target and its centre are parts which are least sputtered and therefore the compound fraction in these areas is very high even for relatively low supply flow of the reactive gas. Different situation occurs at parts with higher values of the discharge current density; those parts of the target are sputtered more effectively so the metal composition of the target is mostly preserved. These target parts are generally called the target racetrack. In the metallic mode, the compound fraction at the racetrack area is very low for both discharge current density profiles – bellow 5 %. The most remarkable change of the target composition takes place during the M-C transition. The compound fraction at the centre of the racetrack is increased dramatically by the M-C transition - for the profile with FWHM 0.02 m by almost 4.5 times and for the profile with FWHM 0.04 m by 3.5 times.

Note that the discharge current density profile is always assumed to be the same in the model, independent of the reactive gas supply flow. Therefore the key variable determining the erosion profile of the target and consequently the target utilization is the profile of the target composition. The relatively flat profile of the compound fraction in the most sputtered area of the target – such as that corresponding to the metallic mode in Fig. 3 – indicates that the target erosion profile and thus the target utili-

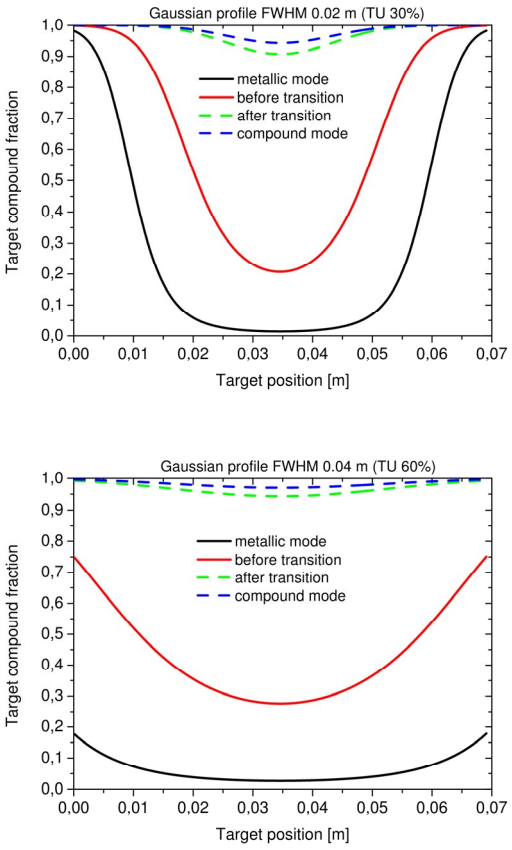

Fig. 3. **Dependency of the compound fraction over the target radius.** Upper and lower graphs correspond to Gaussian profiles of discharge current density with FWHM equal to 0.02 m and 0.04 m, respectively

zation in metallic mode should be only very slightly different from that in the pure metallic mode.

3.2. Modelling of the racetrack shape at different conditions

The target erosion rate can be computed taking into account simultaneously the discharge current density profile and the evolution of the target composition over the target position. The computed target erosion rate was normalized to reach 1 in the most sputtered area of the target in order to compare the racetrack shapes at different process conditions (points B, C, D and E). Moreover, this normalization enables us to visualize the shape of the originally flat target just at the moment when it gets depleted by the sputtering in its racetrack part. Modelled racetrack shape is plotted in Fig. 4. The target utilization can be deduced from modelled racetrack shape of the target.

Fig. 4 shows that the highest target utilization corresponds to the situation when no reactive gas is introduced into the deposition chamber. In that case, the racetrack profile corresponds to the profile of the discharge current density. For a reactive gas introduced into the deposition chamber, the radial evolution of the target composition intervenes in the computation of the racetrack profile.

Different compound fractions of the target are reached for different situations during the sputtering process (see Fig. 3) and the target get sputtered differently too, see Fig. 4. By an increase of the reactive gas supply in the deposition chamber, the target gets progressively covered by the compound mainly in the central parts of the target and at the edges. Since the forming compound is hard to sputter, the profile of the racetrack shrinks. Increasing the reactive gas supply further to higher values, the compound fraction increases even at the racetrack part of the target and the racetrack profile shrinks even more.

For both Gaussian discharge current density profiles, the target utilization is the lowest for the situation shortly before the M-C transition. When the system undergoes the M-C transition, the partial pressure of the reactive gas increases, the target gets almost fully covered by the compound. Although the target erosion rate is lower after M-C transition; resulting profile of the racetrack after the transition is broader than before the transition. For extremely high supplies of the reactive gas, the target is almost fully covered by the compound and the profile of the racetrack is almost identical to the profile of the discharge current density. In that case the target utilization reaches the value corresponding to the pure metallic mode.

For better visualization of the racetrack changes and therefore the changes in the target utilization during the sputtering process evolution, the ratio of the target erosion rates is plotted in Fig. 5 for the Gaussian profile with FWHM = 0.02 m. Values of the target erosion ratio give information on how many times more or less the target is sputtered in the specific position at the target compared to the sputtering in the reference situation. After the addition of the reactive gas, the centre of the target and its edges are

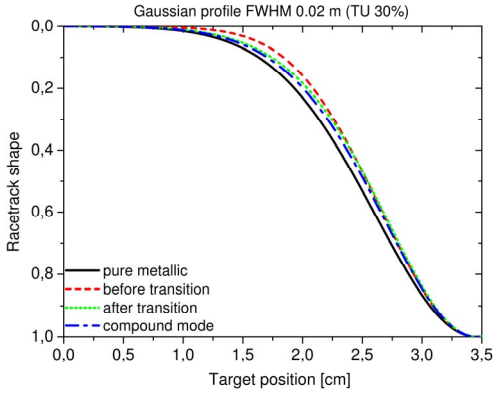

Fig. 4. M**odelled shape of the racetrack in the metallic mode (B), before (C) and after M-C transition (D) and in the compound mode (E).** Upper and lower graphs correspond to Gaussian discharge current density profile with FWHM = 0.02 m and 0.04 m, respectively

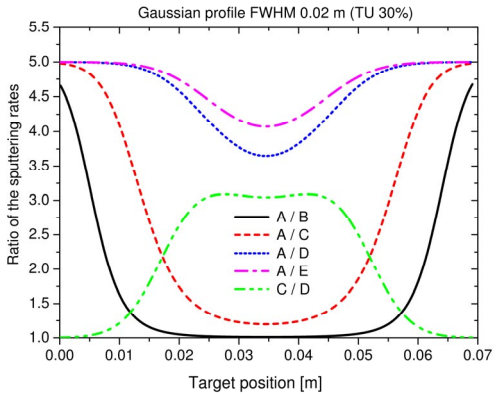

Fig. 5. **Ratio of the target erosion rates at different conditions computed for the Gaussian profile of the discharge current density with FWHM = 0.02 m**

always sputtered 5 times less compared to the pure metallic mode (A) but the racetrack exposed to the relatively high discharge current is sputtered differently depending on the conditions in the reactor. The factor 5 comes from the ratio between the sputtering yield of the metal atom from the clean and from the compound part of the target.

However, more interesting information about the target utilization is provided by the shapes of the ratio plots rather than the absolute values. It is the flatness and the curvature of the plot that is very important for the changes in the target utilization at different process conditions in the reactor. If the ratio of the target erosion rates for two different situations is very flat in the area exposed to a relatively high discharge current density, it means that the target erosion shape is mainly preserved and the target utilization is kept almost the same. This is the case of the ratio plot corresponding to the situation before and after the M-C transition (C/D) for the Gaussian profile with FWHM = 0.02 m in Fig. 5. In this case, the ratio in the racetrack area is around 3, which means that the target material is approximately 3 times less removed from the racetrack than its outer parts from the target centre. But the flatness of the ratio plot indicates that the ratio is the same in the important part of the target. It means that despite the fact that the target at condition corresponding to the point D is depleting about 3 times longer than at the conditions corresponding to the point C; the amount of the target material removed from the target after being depleted at the racetrack is finally approximately the same.

We can conclude that although almost all process parameters change drastically by the transition, the target utilization is not significantly influenced by the transition. In Fig. 5, parts of the curves with high slope point out places where the target erosion rate is changing the most. The continuous compound forming by the reactive gas flow onto the target and its counter effect the continuous sputtering are simultaneous processes resulting in a laterally non-uniform target composition. The progressive shrinking of the racetrack profile with added reactive gas can be well observed from the curved corresponding to A/B and A/C curves in Fig. 5.

3.3. Evolution of the target utilization for different discharge current density profiles

Two particular Gaussian discharge current density profiles with FWHM = 0.02 m and with FWHM = 0.04 m corresponding to the target utilization 30 % and 60 % in the pure metallic mode (point A) were investigated.

Let us investigate the changes in the target utilization in the situation shortly before and shortly after the metallic to compound mode transition as a function of the target utilization magnitude in the pure metallic mode. To quantify the changes in target utilization the Gaussian discharge current density profiles with various target utilization varying from 15 % up to 75 % were modelled by changing the FWHM of Gaussian profile. The changes in the target utilization are expressed as the relative proportion of the target utilization in the studied situation (C and D) to the target utilization in the pure metallic mode (A) for the same discharge current density profile. The ratio of the target utilization in the situation C and D is plotted, too. The results are shown in Fig. 6.

Comparing the situation before the M-C transition with the pure metallic mode the difference in TU is around 8 % independent on the discharge current density profile. If the target is sputtered more economically – in other words by a very broad profile of the discharge current density (TU in the pure metallic mode 50 % or higher) – the changes in the target utilization between the pure metallic mode (A) and the situation after the M-C transition (D) are low, around 5 %. For less economical sputtering by a very sharp and narrow profile of the discharge current density (TU in the pure metallic mode below 30 %) the changes in the target utilization can reach almost 8 %.

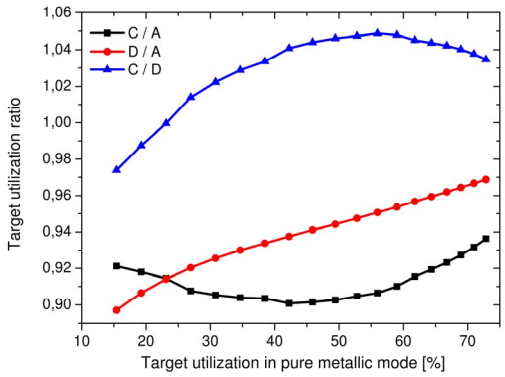

Fig. 6. **The relative proportion of the target utilization in the studied situation (C and D) to the target utilization in the pure metallic mode (A) for various Gaussian discharge current density profiles.** The ratio corresponding to the situation C and D is plotted, too

Comparing the ratio for the situations shortly before and shortly after the M-C transition, it is clear that the transition does not cause any abrupt change in the target utilization. It affects the target utilization maximally by 4 %. Note that the target utilization after the M-C transition is greater than before the transition for all the discharge current density profiles used in practise (those giving the target utilization in the pure metallic mode at least 25 %). Only for very sharp discharge current density profiles, the racetrack shrinking continues even by the transition.

Designed magnetron sputtering source used in practice should have the target utilization in pure metallic mode at least 30–40 %.

4. Conclusion

Changes in the target utilization during the evolution of the magnetron sputtering deposition process were modelled using the extended model of the reactive magnetron sputtering assuming Gaussian discharge current density profiles. The model is a natural extension of the well known Berg model that presumes a uniform discharge current density over the whole target and thus it is not suitable for the investigation of the target utilization.

The role of the target poisoning on the lateral evolution of the target composition and the changes in the racetrack shape with increasing amount of the reactive gas were discussed particularly for two different profiles of the discharge current density. These profiles were chosen to represent the typical magnetic field configuration available on the market – two pole magnetics with target utilization in the pure metallic mode around 30 % and well designed multi pole magnetics that deform and flatten the structure of the magnetic field over the target area to reach the target utilization of 60 %. For both studied profiles, the parts of the target sputtered by low discharge current density are poisoned even for relatively low reactive gas supply flow while the racetrack subjected to high discharge current density is cleaned more effectively by sputtering.

Consequently, the relatively low compound fraction is preserved at the racetrack even for the supplies of the reactive gas close to the supply corresponding to the M-C mode transition. The target poisoning and the target cleaning are continuous and simultaneous processes. The target utilization and the shape of the racetrack for different conditions during the sputtering are modelled and the effect of racetrack shrinking is reported. Shortly before the M-C mode transition the relative compound fraction in the racetrack starts to grow. However, although almost all process parameters change drastically by the M-C transition, the target utilization is not significantly influenced.

To quantify the changes in target utilization for broader range of current density profiles, the Gaussian discharge current density profiles with various target utilization in pure metallic mode varying from 15 % up to 75 % were modelled by changing the FWHM of the Gaussian profile. For the set of the standard input parameters, the differences of the target utilization in the situation shortly before the M-C transition from the pure metallic mode of about 8 % profile were found. This value has been found to be almost independent on the discharge current density profile.

For all studied profiles, the influence of the transition on the target utilization is relatively low – about 4 % – compared to other quantities changing by the transition. Despite that the erosion rate of the target is lower after M-C transition, the resulting profile of the racetracks after the transition is broader than before the transition and consequently the target utilization increases by the transition, too. It could seem surprising that the racetrack does not shrink any more by the transition but it gets broader not realizing that by the transition, the racetrack gets almost fully and equally covered by the compound.

This research has been supported by GACR contracts 104/09/H080, 205/12/0407 and R\&D center project for low-cost plasma and nanotechnology surface modifications CZ.1.05/2.1.00/03.0086 funded by European Regional Development Fund.

REFERENCES

1. Ranjan R., Allain J. P., Hendricks M. R., Rujic D. N.: J. Vac. Sci. Technol. A *19*, 1004 (2001).
2. Tsiogas C. D., Avaritsiotis J. N.: J. Appl. Phys. *71*, 5173 (1992).
3. McMahon R., Affinito J., Parsons R. R.: J. Vac. Sci. Technol. *20*, 376 (1982).
4. Safi I.: Surf. Coat. Technol. *127*, 203 (2000).
5. Schiller S., Heisig U., Goedicke K., Schade K., Teschner G., Hennenberg J.: Thin Solid Films *64*, 455 (1979).
6. Guttler D., Grotzschel R., Moller W.: Appl. Phys. Lett. *90*, 3502 (2007).
7. Moller W., Guttler D.: J. Appl. Phys. *102*, 094501 (2007).
8. Guttler D., Moller W.: Plasma Sources Sci. Technol. *17*, 025016 (2007).
9. Berg S., Blom H.O., Larsson T., Nender C.: J. Vac. Sci. Technol. A *5*, 202 (1987).
10. Berg S., Larsson T., Blom H. O., Nender C.: J. Appl. Phys. *63*, 4267 (1988).
11. Berg S., Nyberg T.: Thin Solid Films *476*, 215 (2005).
12. Larsson T., Blom H.O., Nender C., Berg S.: J. Vac. Sci. Technol. A *6*, 1832 (1988).
13. Kadlec S., Musil J., Vyskocil H.: J. Phys. D: Appl. Phys. *19*, L187 (1986).
14. Musil J., Kadlec S., Vyskocil J., Poulek V.: Surf. Coat. Technol. *39/40*, 301 (1989).
15. Nyberg T., Berg S., Helmersson U., Hartig K.: Appl. Phys. Lett. *86*, 164106 (2005).
16. Kubart T., Kappertz D., Nyberg T., Berg S.: Thin Solid Films *515*, 421 (2006).
17. Vasina P., Hytkova T., Elias M.: Plasma Sources Sci. Technol. *18*, 025011 (2009).

T. Schmidtová and P. Vašina *(Dep. of Physical Electronics, Faculty of Science, Masaryk University, Brno, Czech Republic):* **Modelling of Reactive Magnetron Sputtering with Focus on Changes in Target Utilization**

Target utilization is a parameter determining the usage of the target material for sputtering deposition. It is defined by the relative change in the weight of the target after it becomes depleted at the racetrack by the sputtering. In the case of the sputtering in the non-reactive atmosphere, the target erosion profile copies the profile of the discharge current density. Adding reactive gas into the deposition chamber the target utilization results simultaneously from the discharge current density profile and from the evolution of the target composition. A modified Berg model is used to determine the target utilization during the evolution of the reactive magnetron sputtering deposition process. The shrinking followed by the broadening of the racetrack is reported as the flow of the reactive gas is increased. We quantify these changes in the racetrack profile and the target utilization and we propose a physical interpretation.

ACTIVATION OF SILICON SURFACE IN ATMOSPHERIC OXYGEN PLASMA

DANA SKÁCELOVÁ, PAVEL SŤAHEL, MIRKO ČERNÁK

Department of Physical Electronics, Faculty of Science, Masaryk University, Kotlářská 2, 611 37 Brno, Czech Republic
danka@physics.muni.cz

Keywords: DCSBD, Si wafer, activation, oxygen plasma

1. Introduction

Surface pre-treatment of silicon is a very important process in semiconductor industry. The final properties and utilization of silicon wafers greatly depend on the initial surface conditions[1].

Simple plasma treatment could replace a demanding chemical bath. Various methods, such as Chemical vapor deposition (CVD) or Plasma-enhanced chemical vapor deposition (PECVD)[2] are widely used at present. Nevertheless, the atmospheric pressure plasmas, such as plasma jets[3,4], tend to be appealing in the semiconductor device fabrication.

The aim of this study is to investigate a new technology for plasma treatment of silicon wafer surface. Crystalline silicon surface was treated in Diffuse Coplanar Surface Barrier Discharge (DCSBD) which represents applicable plasma source operating in various gases.

By means of contact angle measurement the modification of c-Si wafers surface with orientation (111) or (100) in oxygen plasma was investigated. Additionally, the effect of orientation and different pre-cleaning procedure were investigated.

2. Experimental setup

Plasma treatment was realized by dielectric barrier discharge in coplanar arrangement, the so-called DCSBD[5–8].

This type of discharge is characterized by the large area of thin layer of atmospheric non – isothermal low temperature plasma on the surface of Al_2O_3 ceramic barrier with embedded metallic electrodes. This geometry ensures the pure plasma without any contaminations from electrodes.

Silicon samples were placed on a movable holder in the discharge chamber in oxygen atmosphere. The discharge chamber was blowen through by oxygen with flow $Q[O_2] = 6$ L min^{-1}.

As a substrate polished n – type, doped with phosphorous, Si (111) having resistivity (33–45)·10^{-3} Ω cm and polished n – type, doped with antimony Si (100) having resistivity (5–18)·10^{-3} Ω cm purchased from ON Semiconductor, Czech Republic,s.r.o. were used.

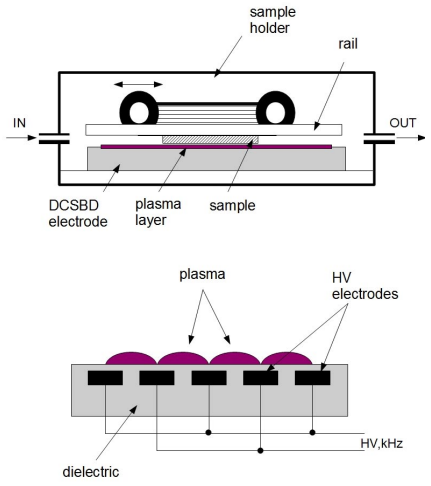

Fig. 1. **Experimental apparatus of DCSBD and the cross section of the electrode**

Before plasma treatment two different cleaning methods were used. The group of samples was cleaned by isopropyl alcohol and cyclohexan (1:1), native oxide layer was retained. Another group of samples was additionally immersed in 1% HF solution for 45 s at the room temperature to remove native oxide layer.

Immediately after cleaning the samples were treated in plasma for 5 s at 350 W.

Contact angle measurements were realized by Surface Energy Evaluation System (SEE System)[9]. Surface free energy γ^{TOT} was calculated by Acid – base model. Water, glycerol and diiodomethane were used as the measuring liquids.

3. Results

The properties of silicon surface before plasma treatment and after plasma treatment are summarized in Tab. I and Tab. II. It is evident that before plasma treatment the water contact angle (WCA) strongly depends on the cleaning procedure and crystallographic orientation of silicon. Etching in HF solution makes the surface more hydrophobic due to H terminating of dangling bonds.

However, after plasma treatment WCA markedly decreased to less than 5° independently on the orientation

Table I
Surface properties of the silicon samples before plasma treatment

	WCA	γ^{TOT}	γ^{LW}	γ^{AB}
(100) IPA cleaned	38.6	56.7	41.0	15.5
(100) HF etched	84.6	48.8	47.9	0.9
(111) IPA cleaned	38.7	53.8	36.3	17.5
(111) HF etched	65.6	52.3	45.9	6.4

and cleaning process. The improving of wettability after plasma treatment is caused by creating hydroxyl OH groups on the surface, which are responsible for hydrophilic properties of silicon[10]. This fact was successfully confirmed due to increasing of acid-base component γ^{AB} of surface free energy in case of all investigated samples (Tab. II).

Table II
Surface properties of the silicon samples after plasma treatment

	WCA	γ^{TOT}	γ^{LW}	γ^{AB}
(100) IPA cleaned	4.5	60.4	42.5	17.8
(100) HF etched	3.5	62.5	42.7	19.7
(111) IPA cleaned	5.6	61.5	42.7	18.8
(111) HF etched	4.0	61.8	42.5	19.4

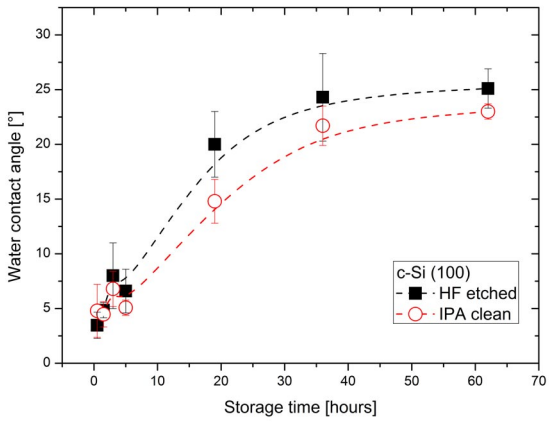

Fig. 2. **Ageing effect of treated c-Si (100)**

Moreover, the ageing effect of oxygen plasma modification was investigated. Fig. 2 and Fig. 3 show the change of water contact angle for (100) and (111) oriented plasma treated c-Si samples during exposure to ambient condition. In principle, within about one day the water

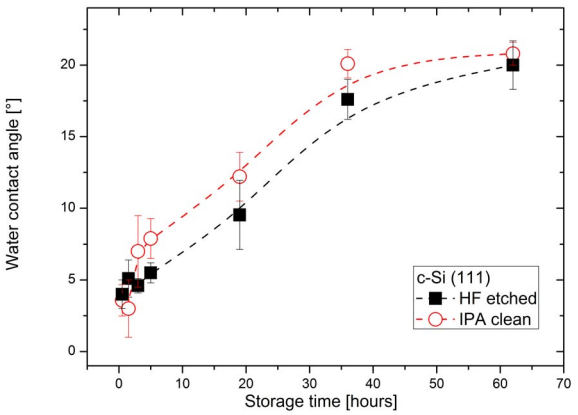

Fig. 3. **Ageing effect of treated c-Si (111)**

contact angle achieved the value that changed further slightly. All samples tend to achieve almost the same constant value of WCA within 40 hours. This phenomenon is caused by the loss of OH groups on the surface and adsorption of contamination from air.

5. Conclusion

In the current work, the modification of silicon surface wafer in oxygen atmospheric plasma was studied. DCSBD was used to plasma modification of crystalline silicon samples in orientation (111) and (100) and different pre-cleaning process. Furthermore, the ageing effect of plasma treated samples was studied.

Contact angle measurement proved the appreciable improving of wettability after plasma treatment independent on crystallographic orientation of cleaning process.

This research has been supported by the project R&D center for low-cost plasma and nanotechnology surface modifications CZ.1.05/2.1.00/03.0086 funded by European Regional Development Fund.

REFERENCES

1. Siffert P., Krimmel E. : *Silicon: evolution and future of a technology*. Springer-Verlag, Berlin 2004.
2. Rossnagel S. M., Westwood, W. D., Cuomo J. J.: *Handbook of Plasma Processing Technology: Fundamental, Etching, Deposition and Surface Interactions*. Noyes Publication, New York 1989.
3. Habib S. B., Gonzales E., Hicks R. F.: J. Vac. Sci. Technol. *A 28*, 476 (2010).
4. Dani I., Mäder G., Grabau P., Dresler B., Linaschke D., Lopey E., Kaskel S., Beyer E. : Contrib. Plasma Phys. *49*, 662 (2009).
5. Šimor M., Ráhel´ J., Vojtek P., Černák M., Brablec

A.: Appl. Phys. Lett. *81*, 2716 (2002).
6. Skácelová D., Sťahel P., Haničinec M., Černák M.: Acta Tech. *56*, T356 (2011).
7. Buček A., Homola T., Aranyosiová M., Velič D., Plecenik T., Havel J., Sťahel P., Zahoranová A.: Chem. Listy *102*, 1459 (2008).
8. Černáková L., Szabová R., Wolfová M., Buček A., Černák M.: Fibres Text. East. Eur. *15(5-6)*, 121 (2007).
9. Buršíková V., Sťahel P., Navrátil Z., Buršík J., Janča J.: *Surface Energy Evaluation of Plasma Treated Materials by Contact Angle Measurement*. Masaryk university, Brno 2004.
10. Zhang X. G.: *Electrochemistry of Silicon Surface and Its Oxide*. Kluwer Academic Publisher, New York 2003.

D. Skácelová, P. Sťahel, and M. Černák *(Department of Physical Electronics, Faculty of Science, Masaryk University, Brno, Czech Republic):* **Activation of Silicon Surface in Atmospheric Oxygen Plasma**

In this contribution, the surface modification of crystalline silicon surface in oxygen atmosphere was investigated. Moreover the effect of crystallographic orientation and surface pre-cleaning of silicon surface were studied. c-Si wafers (100) and (111) oriented were cleaned in isopropyl alcohol or etched in HF solution and afterwards treated in Diffuse Coplanar Surface Barrier Discharge.

Wettability, changes of surface properties and ageing effect of plasma treated surface were studied by means of contact angle measurement.

It was proved that modification of c-Si surface in oxygen plasma improves the wettability independently on crystallographic orientation and initial cleaning process.

MECHANICAL STABILITY OF THE P-I-N SOLAR CELLS STUDIED BY INDENTATION METHOD

VILMA BURŠÍKOVÁ[a,b], PETR SLÁDEK*[c], PAVEL SŤAHEL[a]

[a] Department of Physical Electronics, Faculty of Science, Masaryk University, Kotlářská 2, 611 37 Brno, [b] CEITEC, Central European Institute of Technology, Masaryk University, 601 77 Brno, [c] Department of Physics, Chemistry and Vocational Education Faculty of Education, Masaryk University, Poříčí 7, 603 00 Brno, Czech Republic
sladek@jumbo.ped.muni.cz

Keywords: solar cells, mechanical stability, hardness, elastic modulus, interfacial fracture toughness

1. Introduction

The mechanical stability of the solar cells may play a crucial role in their technological application and their determination is of great importance. One of the most suitable methods of characterization of mechanical properties of thin films is the indentation technique. Besides the film hardness, the method also enables to determine also other important material properties such as the film elastic modulus, the plastic and elastic part of the indentation work, the fracture toughness of the film and the film substrate interface.

The aim of the present work was to describe the determination of the above listed parameters for typical p-i -n silicon solar cells.

2. Experimental part

The studied p-i-n solar cells were deposited by RF glow discharge in ARCAM reactor[1]. In Fig. 1 the structure of the studied solar cells is shown. The solar cells consist of several layers. At first, an about 10 nm thick p-doped a-SiC:H layer was deposited, followed by 10 nm thick a-SiC:H layer and 12 nm thick standard buffer a-Si:H layer. The subsequent thick intrinsic i(a-Si:H) layer and the following 12 nm thick buffer a-Si:H layer was finally coated by a 20 nm thick n-doped n(a-Si:H) layer. All layers were deposited at 180 °C.

In case of the structured coatings, the interfacial fracture toughness of the particular interfaces is one of the most important parameters for the mechanical stability of the solar cells.

The depth sensing indentation (DSI) method by means of Fishercope H100 tester, equipped with Vickers indenter was used for determination of the mechanical properties of the films. In the case of the Fischerscope H100 tester the applied load is registered as a function of indentation depth both during loading and unloading. The maximum applied load could be changed in the range from 1 mN to 1 N. The sensitivity of the depth measurement is approximately ± 1 nm. In order to minimize the experimental errors, each measurement was repeated at least 9 times.

On the basis of the DSI method the universal hardness *HU* (also called Martens hardness *HM*) as a measure of the material resistance against elastic and plastic deformation may be obtained. *HU* is calculated as the contact pressure (ratio of the applied load *L* to the immediate contact area *A*). In our case, the Vickers technique based on the indentation of square-based diamond pyramid with face angle $\alpha = 136°$ was used. The so called plastic hardness HU_{pl} is obtained as the ratio of the maximum applied load and the area of the remained indentation print A_d. The loading and unloading curves enable to determine the elastic and plastic part of the indentation work (W_e and W_{pl}), the effective elastic modulus $Y = E/(1–\nu^2)$, where E is the Young's modulus and n is the Poisson's ratio of the films and the hardness of the film[2].

The indentation may introduce substantial cracks and adhesive failures into the thin films. By the analysis of the morphology of the indentation prints, it is possible to determine material characteristics as the fracture toughness of the films and the resistance of the film-substrate interface against delamination. The fracture toughness of the coating-substrate interface could be estimated from the analysis of the energy dissipated during the indentation[3]. During the deformation, the total deformation work is transformed into elastic strain energy W_{el}, energy dissipated due to plastic deformation W_{pl}, energy dissipated due to fracture W_{fr} and thermal energy W_{th}. The area between

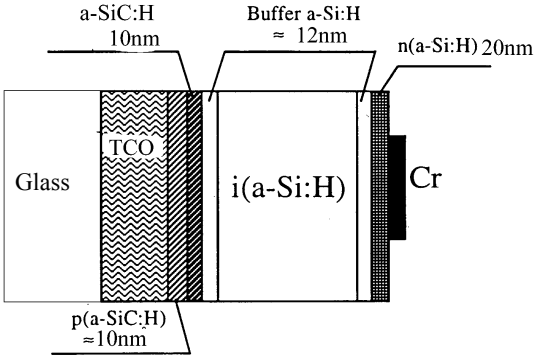

Fig. 1. **Schema of the studied solar cells**

the loading and unloading curves gives the total amount of the dissipated energy. The energy dissipated in the propagation of the delamination crack can be related to the interfacial fracture energy W_{fr}. The interfacial energy release rate G_{int} can be obtained on the basis of the indentation work W_{fr} needed for creation of delaminated area with radius c (Fig. 1). The interfacial fracture toughness K_{int} was calculated according to the following formulas:

$$G_{\text{int}} = \frac{W_{fr}}{\pi c^2}, \quad \frac{1}{E_{\text{int}}} = \frac{1}{2}\left(\frac{1}{E_f} + \frac{1}{E_s}\right) \tag{1}$$

$$K_{\text{int}} = \sqrt{G_{\text{int}} E_{\text{int}}} \tag{2}$$

Here E_{int} is the so called interfacial elastic modulus defined by Hutchinson and Suo[4]. E_f is the film elastic modulus and E_s the substrate elastic modulus.

The morphology of the film surface and the indentation prints was studied by means of Zeiss – Neophot optical microscope, a Nicon SMZ - 2T optical stereomicroscope, a Philips SEM 505 scanning electron microscope and by AFM.

3. Results and discussion

The analysis of the load-penetration curves was done for several p-i-n solar cells with different thicknesses. Because of the complicated structure of the solar cells the measurements were made for several different indentation depths (i.e. several different applied loads) in order to map the mechanical properties from near surface up to film-substrate interface.

In Fig. 2 the load-penetration curves carried out at maximum load L = 10 mN for 3.4 μm thick p-i-n solar cell

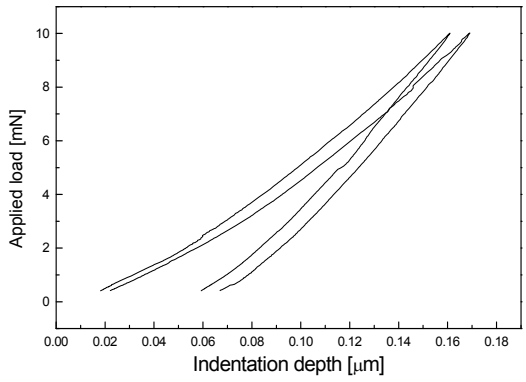

Fig. 2. **Load-penetration curves measured for 3.4 μm thick p-i-n solar cell.** The maximum load was L = 10 mN

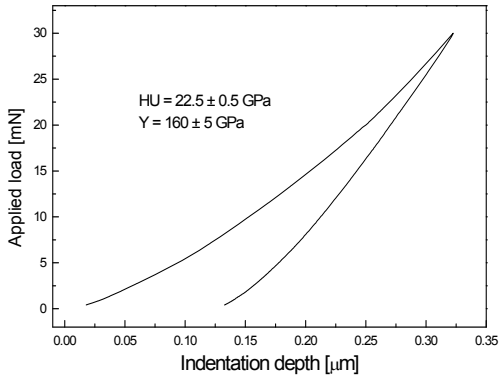

Fig. 3. **Load-penetration curves measured for 3.4 μm thick p-i-n solar cell.** The maximum load was L = 30 mN. The loading and unloading time was 60 s

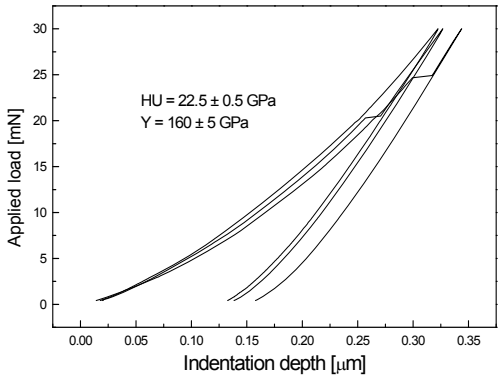

Fig. 4. **Load-penetration curves measured for 3.4 μm thick p-i-n solar cell.** The maximum load was L = 30 mN. The loading and unloading time was 20 s

are shown. The time of the loading and unloading was t = 20 s. The measured plastic hardness HU_{pl} was 25 ± 5 GPa, the universal hardness was 7.7 ± 0.7 GPa and the elastic modulus 160 ± 10 GPa. The load-penetration curves and the experimental values were scattered due to the interfacial effects such as interfacial microcracks. The effect of microcracks could be observed in Fig. 2 as jumps on the curve. These microcracks were created at the first two interfaces between the n-doped a-Si:H and the buffer a-Si:H layer or between the buffer layer and the intrinsic layer.

With increasing loading time, i.e. decreasing deformation rate, the cracks were not created. This effect was observed also for higher applied loads. An example is shown in Fig. 3. The maximum load was 30 mN and the loading time was 60 s. The universal hardness was

7.7 ± 0.5 GPa. The plastic hardness HU_{pl} was 22.5 ± 0.5 GPa and the elastic modulus was $Y = 160 \pm 5$ GPa. The load penetration curves made with low deformation rate were smooth without jumps as it is shown in Fig. 3. On the other hand high deformation rates (loading time $t = 20$ s) caused sudden deformations appearing on the load-penetration curve as jumps. This effect is shown in Fig. 4. The maximum applied load was the same as in Fig. 3. These jumps indicate sudden slips or creation of microcracks at the interface. At higher loads (higher indentation depths) the jumps appear also at low deformation rates due to the influence of the bottom interfaces.

At higher applied loads the 0.9 μm thick solar cell showed also the indentation induced delamination around the indentation prints. In Fig. 8 the indentation prints made at 0.5 N are shown. Due to film transparency there is clearly shown the indentation induced separation (delamination) of the film from the substrate at the film-substrate interface.

Measuring the radius of the delaminated area, we can determine the fracture toughness of the film-substrate interface according to equations (*1*) and (*2*). The calculated interfacial fracture toughness of the 0.9 μm thick solar cell was $K_{ic} = 7.2 \pm 0.5$ MPa $m^{1/2}$.

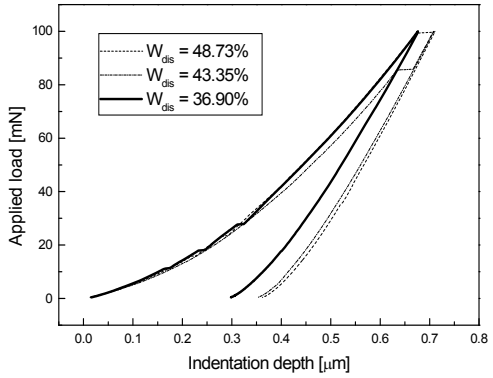

Fig. 5. **Load-penetration curves measured for 3.4 μm thick p-i-n solar cell.** The maximum load was L=100 mN. The loading and unloading time was 60 s. In the graph the total irreversibly dissipated parts of deformation work are given in percents

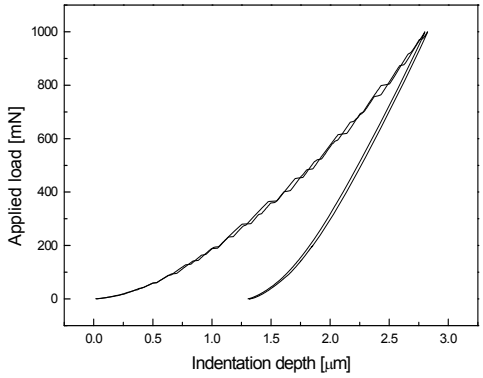

Fig. 6. **Load-penetration curves measured for 3.4 μm thick p-i-n solar cell.** The maximum load was L = 1 N. The loading and unloading time was 60 s

Table I
Determination of the deformation work made with applied load 100 mN. W_{tot} is the total, W_{el} is the elastic and W_{ird} is the irreversibly dissipated work. W_{int} is the work for interfacial deformation

W_{tot} [nJ]	W_{el} [nJ]	W_{ird} [nJ]	W_{int} [nJ]
26.6	16.8	9.8	~0
27.0	16.5	10.5	0.7
27.1	16.3	10.7	0.9
28.1	15.9	12.2	2.4
30.2	15.5	14.7	4.9

The DSI technique enables us to quantitatively determine the indentation work, which was needed for the plastic, elastic and interfacial deformation. The determination of the particular parts of the total indentation work is shown in Fig. 5.

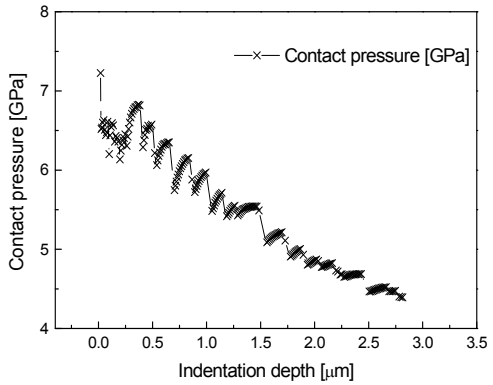

Fig. 7. **The dependence of the contact pressure between the indenter and the thin film-substrate system on the indentation depth measured for 3.4 μm thick p-i-n solar cell.** The maximum load achieved at the end of the loading was L = 1 N. The loading and unloading time was 60 s

4. Conclusion

The depth sensing indentation technique was used for characterization of the mechanical properties of the p-i-n solar cells. Cells of several different thicknesses were studied. Detailed analysis of load-penetration curves obtained at applied loads ranging from 10 to 1000 mN and for two deformation rates was done. The determination of important material parameters such as plastic and universal hardness, elastic modulus, the irreversibly dissipated deformation work and the interfacial fracture toughness was shown. The possible deformation mechanism of structured thin films resulting loading curves by steps was described.

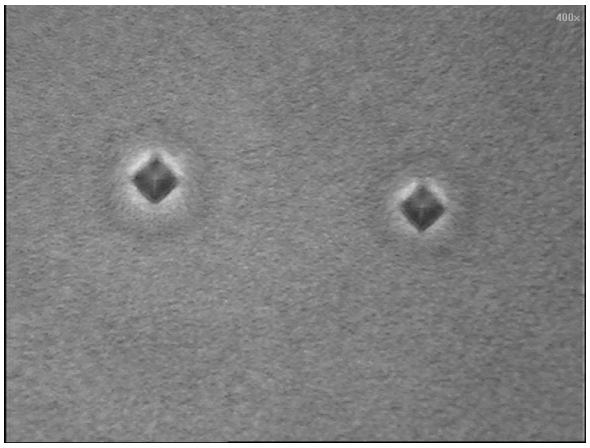

Fig. 8. **Optical micrographs of the indentation prints made in the 0.9 μm thick solar cell with applied load L = 0.5 N**

This research was supported by the Grant Agency of the Academy of Sciences of the Czech Republic under contract KAN311610701 and by the project CZ.1.05/2.1.00/03.0086 'R&D center for low-cost plasma and nanotechnology surface modifications' funded by European Regional Development Fund.

REFERENCES

1. Roca i Cabarrocas P., Chévrier J. B., Huc J., Loret A., Parey J. Y., Schmitt J. P. M.: J. Vac. Sci. Technol. *A9*, 2331 (1991).
2. Pharr G. M., Oliver W. C., Brotzen F. R.: J. Mater. Res. *7*, 613 (1992).
3. Malzbender J., et.al.: Mater. Sci. Eng. R *36*, 47 (2002).
4. Hutchinson J. W., Suo Z.: Adv. Appl. Mech. *29*, 63 (1992).

V. Buršíková[a,b], P. Sládek[c], and P. Sťahel[a]
([a] Department of Physical Electronics, Faculty of Science, Masaryk University, Brno, [b] CEITEC, Central European Institute of Technology, Masaryk University, Brno, [c] Department of Physics, Chemistry and Vocational Education Faculty of Education, Masaryk University, Brno, Czech Republic): **Mechanical Stability of the P-I-N Solar Cells Studied by Indentation Method**

The main priorities when preparing the p-i-n amorphous silicon based solar cells are the efficiency as well as the optoelectronic stability of the cells. However, for the final applications, a good mechanical and thermomechanical stability is not of the second order of importance. The large internal mechanical stress, weak adhesion can result the deterioration of the solar cell (cracking, delamination).

The objective of our study was to investigate the mechanical properties of p-i-n amorphous silicon based solar cells by means of depth sensing indentation technique (Fisherscope H100). The instrumented indentation method combined with the study of the morphology of the indentation prints enable us to determinate microhardness, fracture toughness of the interface with substrate and internal stress.